

# Turbidites, topography and tectonics: Evolution of submarine channel-lobe systems in the salt-influenced Kwanza Basin, offshore Angola

Danielle M. Howlett<sup>1</sup>  | Rob L. Gawthorpe<sup>1</sup>  | Zhiyuan Ge<sup>1</sup>  | Atle Rotevatn<sup>1</sup>  | Christopher A.-L. Jackson<sup>2</sup> 

<sup>1</sup>Department of Earth Science, University of Bergen, Bergen, Norway

<sup>2</sup>Basins Research Group (BRG), Department of Earth Science & Engineering, Imperial College, London, United Kingdom

## Correspondence

Danielle M. Howlett, Department of Earth Science, University of Bergen, Bergen, Norway.

Email: danielle.howlett@uib.no

## Funding information

Equinor

## Abstract

Understanding the evolution of submarine channel-lobe systems on salt-influenced slopes is challenging as these systems react to subtle, syn-depositional changes in sea-floor topography. The impact of large blocking structures on individual deep-water systems is well documented, but our understanding of the spatial and temporal evolution of extensive channel-lobe systems on slopes influenced by relatively modest salt structures is relatively poor. We focus on Late Miocene deep-water depositional systems contained within a c. 450 ms TWTT thick interval imaged in 3D seismic reflection data from the contractional salt-tectonic domain, offshore Angola. Advanced seismic attribute mapping, tied to seismic facies analysis and time-thickness variations, reveal a wide range of interactions between structurally induced changes in slope relief, deep-water sediment routing, geomorphology and sedimentology. Five seismic units record a striking tectono-stratigraphic within eight minibasins. We observe gradual channel diversion through lateral migration during times of relatively high structural growth rate, as opposed to abrupt channel movement via avulsion nodes during times of relatively high sediment accumulation rate. Our models capture the response of deep-water depositional systems to the initiation, maturation, and decay of contractional structures on salt-influenced slopes. The initiation stage is defined by small, segmented folds with deep-water depositional system being largely able to transverse multiple minibasins. In contrast, the maturity stage is characterised by large, now-linked high-relief structures bounding prominent minibasins leading to ponding and large-scale diversion of channel-lobe systems and the emplacement of MTCs derived from nearby highs. The decay stage is expressed by structures that are shorter and more subdued than those characterising the maturity stage; this leads to a more complicated array of channel-lobe system, the evolution of which is still influenced by bypass, diversion and ponding. During the decay stage, remnant structures still exert a subtle but key control on the development and positioning of avulsion nodes.

This is an open access article under the terms of the Creative Commons Attribution License, which permits use, distribution and reproduction in any medium, provided the original work is properly cited.

© 2020 The Authors. *Basin Research* published by International Association of Sedimentologists and European Association of Geoscientists and Engineers and John Wiley & Sons Ltd

**KEYWORDS**

deep-water turbidite systems, Kwanza Basin, minibasins, salt tectonics, seismic geomorphology, turbidite channels and lobes

## 1 | INTRODUCTION

Sea-floor topography has a significant impact upon turbidity currents and their associated deposits. Structurally controlled sea-floor topography that influences deep-water gravity flows may be due to underlying normal faults (e.g. Ge, Nemec, Gawthorpe, Rotevatn, & Hansen, 2018; Haughton, 2000; Mattos, Alves, & Scully, 2019; Muravchik et al., 2019), thrusts with fault-propagation folds (e.g. Clark & Cartwright, 2012; Howlett et al., 2019; Jolly, Lonergan, & Whittaker, 2016; Jolly, Whittaker, & Lonergan, 2017; Pinter et al., 2018; Tinterri, Laporta, & Ogata, 2017) or salt-cored structures (e.g. Hay, 2012; Mayall et al., 2010; Oluboyo, Gawthorpe, Bakke, & Hadler-Jacobsen, 2014). In addition, pre-existing sedimentary features may have an expression on the sea-floor, such as differential compaction of stacked channels (e.g. Ward, Alves, & Blenkinsop, 2017) and mass transport deposits (e.g. Ortiz-Karpp, Hodgson, & Mccaffrey, 2015; Zhao, Qi, Patacci, Tan, & Xie, 2019). Structurally controlled sea-floor topography may result in turbidity current-fed systems being deflected, diverted, constricted or blocked (Clark & Cartwright, 2009; Kneller & McCaffrey, 1995; Oluboyo et al., 2014; Prather, Booth, Steffens, & Craig, 1998). Deep-water systems can experience diversion for kilometres around long, high-amplitude folds (Mayall et al., 2010), or structural constriction when forced through narrow spill-points between structural highs, such as a segment boundary between two co-linear folds (Oluboyo et al., 2014; Patacci, Haughton, & Mccaffrey, 2015). Deep-water systems are blocked when confining topography traps the deep-water flows thereby creating a suspension cloud resulting in 'flow ponding' (Van Andel & Komar, 1969). Additional complicating factors include the angle of incidence with topography, internal flow parameters, such as grain size, density and stratification, as well as relative scaling between the height of the flow and the obstacle. These variable flow parameters influence fluid dynamics and resulting sediment deposition, and have been systematically modelled in flume tank experiments and numerical models (e.g. Kneller, Edwards, Mccaffrey, & Moore, 1991; Kneller, 1995; Eggenhuisen & McCaffrey, 2012; Cartigny, Eggenhuisen, Hansen, & Postma, 2013; Aas et al., 2014; Basani et al., 2014; Howlett et al., 2019). These concepts are applicable for individual flows but can also be extended to consider the accumulated effect of potentially thousands of these flows that build stratigraphic successions of the type and thickness observable in seismic reflection data. The behaviour of turbidite-fed deep-water systems in structurally

**HIGHLIGHTS**

- Tectono-stratigraphic evolution of Late Miocene salt minibasins on the Angolan continental margin.
- The variable response of submarine deep-water channel-lobe systems to complex, structurally controlled sea-floor topography.
- The interplay of structural growth rate and sediment accumulation rate in altering the geomorphology and routing of channel-lobe systems.
- Models showing the development of deep-water depositional systems in contractional salt domains during initiation, maturity and decay stages of structural evolution.

active regions can be very complex given both the sea-floor topography and depositional systems themselves can vary spatially due to syn-depositional growth of intra-basinal structures, changes in sediment supply, routing and flow size relative to these structures (e.g. Liu, Kneller, Fallgatter, Valdez Buso, & Milana, 2018). Consequently, understanding the detailed sedimentological response of extensive submarine channel-lobe systems to complex sea-floor topography, particularly in regions with mobile shale or salt substrates, remains challenging.

Regions with mobile salt substrate and deep-water systems include well-studied basins in the Gulf of Mexico (Smith, 2004; Prather et al., 2012), eastern Mediterranean Levant Basin (Clark & Cartwright, 2009; Niyazi et al., 2018), offshore Brazil, such as the Santos or Espirito Santo Basins (Gamboa & Alves, 2015; Rodriguez, Jackson, Bell, Rotevatn, & Francis, 2020), as well as along the west African margin, such as the Lower Congo or Kwanza Basins (Broucke et al., 2004; Oluboyo et al., 2014). Large-scale tectonic studies often utilise regional 2D seismic reflection data to understand structural development (Marton, 2000; Valle, Gjelberg, & Helland-Hansen, 2001; Tari et al., 2003; Hudec & Jackson, 2004), and these have developed useful methods to analyse the geometry of stratal packages deposited next to mature passive diapirs in local studies (Giles & Rowan, 2012; Pichel, Jackson, Peel, & Dooley, 2020; Rojo & Escalona, 2018). Tectono-stratigraphic studies often focus on the mature stages of structural growth, as this is when the influence of salt-cored structures, such as ponding and blocking,

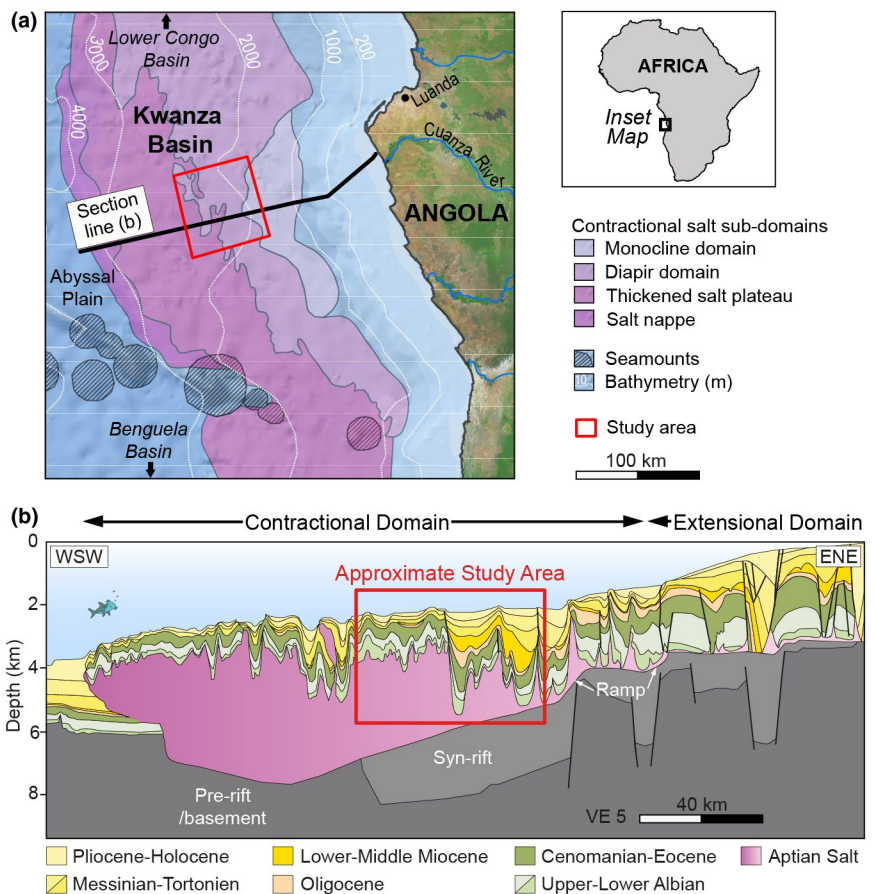
most drastically affect turbidite systems. Conversely, the impact during fold decay has often been underestimated. The intricate evolution of deep-water systems is well imaged in high-resolution 3D seismic reflection data through seismic attribute analysis. Most emphasis has been on the sedimentological response of individual channel-levee systems around solitary salt-cored structures (e.g. Clark & Cartwright, 2009; Gee & Gawthorpe, 2006; Gee, Gawthorpe, Bakke, & Friedmann, 2007), with recent studies of the responses of lobe complexes to diapiric growth (Doughty-Jones, Mayall, & Lonergan, 2017). Less attention has been devoted to the combination of these depositional elements (i.e. channel-lobe complexes) and on controls over the transitional zone between confined to unconfined flows, often referred to as channel-lobe transition zone (CLTZ; Mutti & Normark, 1991; Brooks, Hodgson, Brunt, Peakall, Hofstra & Flint, 2018; Hofstra, Hodgson, Peakall, & Flint, 2015; Wynn, Kenyon, Masson, Stow, & Weaver, 2002). There has been increasing interest in controls over the locations for newly formed channel pathways, referred to as avulsion nodes (Armitage et al., 2012), as these are key for understanding exactly how channels move as structures grow and why some channels shift abruptly via these nodes whereas others migrate laterally more gradually.

In this study, we use an extensive 3D seismic reflection survey to complete a detailed tectono-stratigraphic analysis

of a series of minibasins in the Kwanza Basin, c. 100 km offshore Angola. The stratigraphic interval of interest is within the Miocene and is composed of >50 km long submarine channel-lobe systems trending both transversely and axially to structural strike. We aim to document the effect of salt-influenced sea-floor topography on the routing and geomorphology of submarine channel-lobe systems. Specific objectives include (s) to understand the location and character of transition zones between depositional elements (i.e. CLTZ, avulsion nodes) in relation to sea-floor topography, and (b) to develop a model for the evolution of channel-lobe systems that incorporates the different stages in the growth of salt-cored folds.

## 2 | GEOLOGICAL SETTING AND STUDY AREA

The focus of this study, the northern Kwanza Basin, is bounded to the north by the Lower Congo Basin and to the south by the WNW-trending Cretaceous Kwanza seamounts (Figure 1a; Guiraud, Buta-Neto, & Quesne, 2010; Marton, 2000). Similar to other sedimentary basins along the West African margin (offshore Gabon, Congo, Angola and Namibia), the Kwanza Basin formed during rifting and break-up of the Gondwana supercontinent in the Late Jurassic to



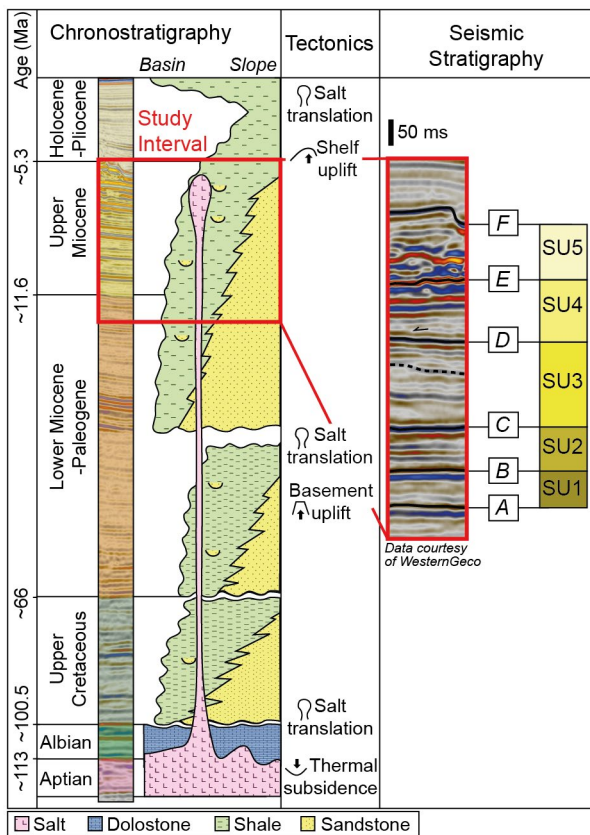
**FIGURE 1** (a) Simplified contractional salt domains in the Kwanza Basin, offshore Angola with the study area outlined (modified after Hudec & Jackson, 2004; additions from Tari et al., 2003; Serié, Huuse, Schødt, Brooks, & Williams, 2017). (b) Geological cross-section showing the regional tectono-stratigraphic framework through the Kwanza Basin (from Hudec & Jackson, 2004). The study area is within the contractional domain containing salt-cored structures such as salt stocks and walls up-dip, and a thickened salt plateau down-dip. Within this area the Miocene is thick in the east and thins westwards onto the thickened salt

Early Cretaceous (Brice, Cochran, Pardo, & Edwards, 1982; Guiraud et al., 2010; Guiraud & Maurin, 1992; Jian-Ping et al., 2008; Karner & Driscoll, 1999; Moulin et al., 2005).

The stratigraphy of the Kwanza Basin can be divided into pre-salt (Late Proterozoic-Barremian), salt (Aptian) and post salt mega-sequences (Albian-present). The pre-salt sequence is comprised mostly of continental deposits contained within intracratonic rift basins. A post-rift sag basin developed during the Barremian and restricted marine conditions during the Aptian led to the deposition of evaporites that are, on average, 3 km thick in the offshore Kwanza Basin (Hudec & Jackson, 2004). The initial deposits of the post-salt sequence (Albian) were predominately shallow water carbonates, followed by clastic progradation and deep-water sedimentation (Cenomanian-Eocene; Anderson, Cartwright, Drysdall, & Vivian, 2000; Brownfield & Charpentier, 2006; Lavier, Steckler, & Brigaud, 2001; Valle et al., 2001). Tectonic uplift and tilting of the margin resulted in shelf erosion and sediment delivery to deep-water channel-lobe systems (Miocene-Oligocene; Figure 2; Anderson et al., 2000; Brice et al., 1982; Jackson, Hudec, & Hegarty, 2005). During the Pliocene through to present, low sediment influx and relatively high

sea level resulted in the deposition of dominantly hemipelagic clays and silts with channel-lobe systems restricted to areas of the Kwanza Basin down-dip of major river mouths (Figure 2).

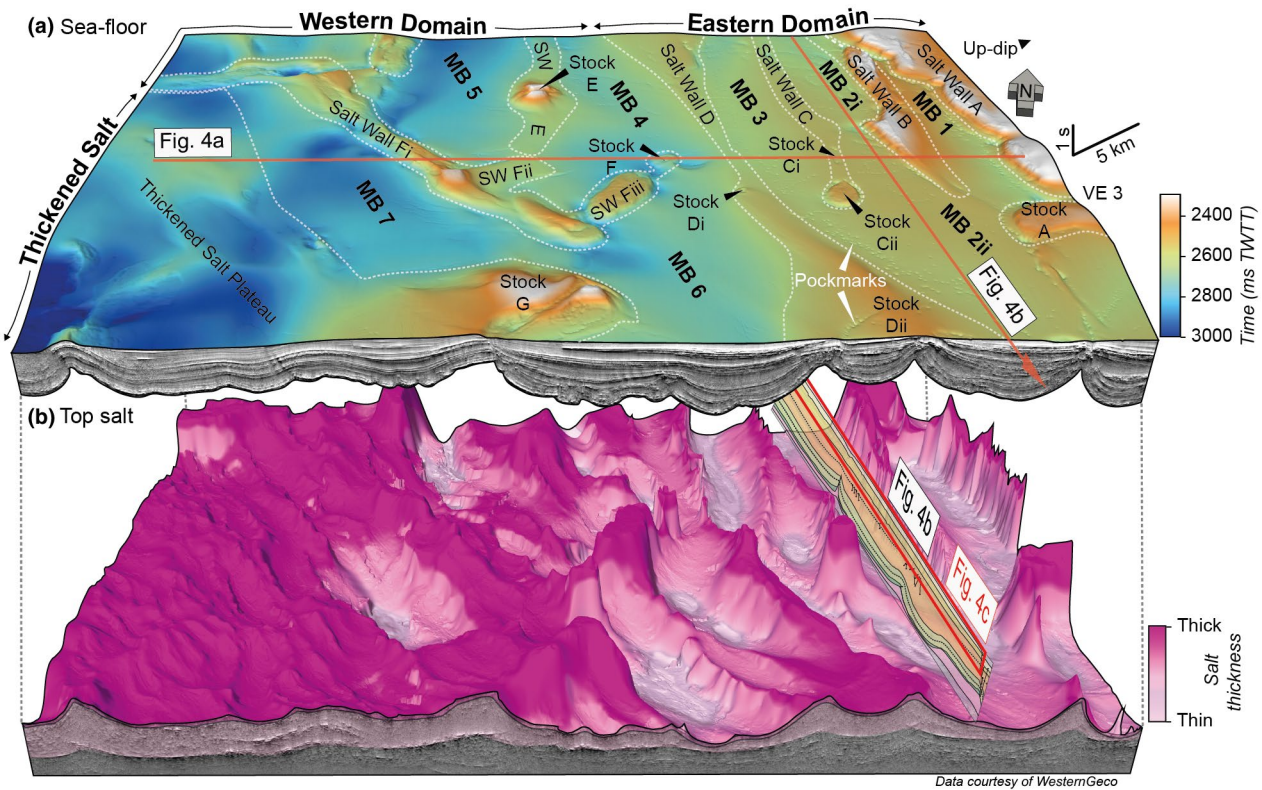
The structural style of the post-salt mega-sequence is gravity-driven thin-skinned deformation creating an up-dip extensional domain along the shelf and proximal slope, which is kinematically linked to a down-dip contractional domain (Marton, 2000; Valle et al., 2001; Fort, Brun, & Chauvel, 2004; Brun & Fort, 2011; Quirk et al., 2012). Salt-related deformation preserved on the present-day sea-floor began shortly after the deposition of the Albian carbonates continuing until the present, with several periods of salt flow and growth of related structures (Figures 2 and 3; Duval, Cramez, & Jackson, 1992). Within the extensional domain listric growth faults, grabens and rafts dominate, whereas the contractional domain contains mostly thrusts with fault-propagation folds, salt nappes, and squeezed diapiric salt stocks and walls (Duval et al., 1992; Lundin, 1992; Tari et al., 2003; Guiraud et al., 2010). We differentiate salt stocks and walls based on their planform geometry; that is, salt stocks are broadly circular (length:width <3), whereas salt walls are more elongate (length:width >3; Hudec & Jackson, 2007). Many contractional structures trend parallel to the shelf break due to gravitational gliding of the mobile substrate (Peel, 2014). The regional line from Hudec and Jackson (2004) suggests there are considerable base-salt steps in the Kwanza Basin, several of which lie directly east of the study area (Figure 1b). The African continental margin and these basement steps were uplifted around the Late Miocene (8 Ma) and likely influenced the ramp-syncline basin style of sedimentary fill observed within the older stratal packages of some minibasins in the study area (Pichel, Finch, & Gawthorpe, 2019; Pichel, Peel, Jackson, & Huuse, 2018).



**FIGURE 2** Simplified Upper Jurassic to Quaternary stratigraphy of the Kwanza Basin and main tectonic events (modified after Serié et al., 2017). Note the multiple events reviving salt translation. The five seismic units with corresponding seismic character are displayed on the right-hand side

### 3 | DATA AND METHODOLOGY

The study utilises a time-migrated 3D seismic reflection survey collected within the Kwanza Basin in water depths between 1800 m and 2300 m (Figure 1a). The study area is within the down-dip contractional salt domain, defined by salt walls and stocks separating intraslope minibasins (Figures 1b and 3). The eastern edge of the survey is c. 30 km down-dip of the Late Miocene base-of-slope (Hudec & Jackson, 2004). The seismic survey covers c. 3,500 km<sup>2</sup>, with a 4-ms sample interval and a crossline and inline spacing of 12.5 and 25 m, respectively. The data are processed and displayed as zero phase, with a positive impedance contrast represented as a peak (blue reflection in presented seismic images). No well calibration is available and stratigraphic age is based on correlation to regional lines (Hudec & Jackson, 2004) and nearby interpretations (Oluboyo et al., 2014). Data quality



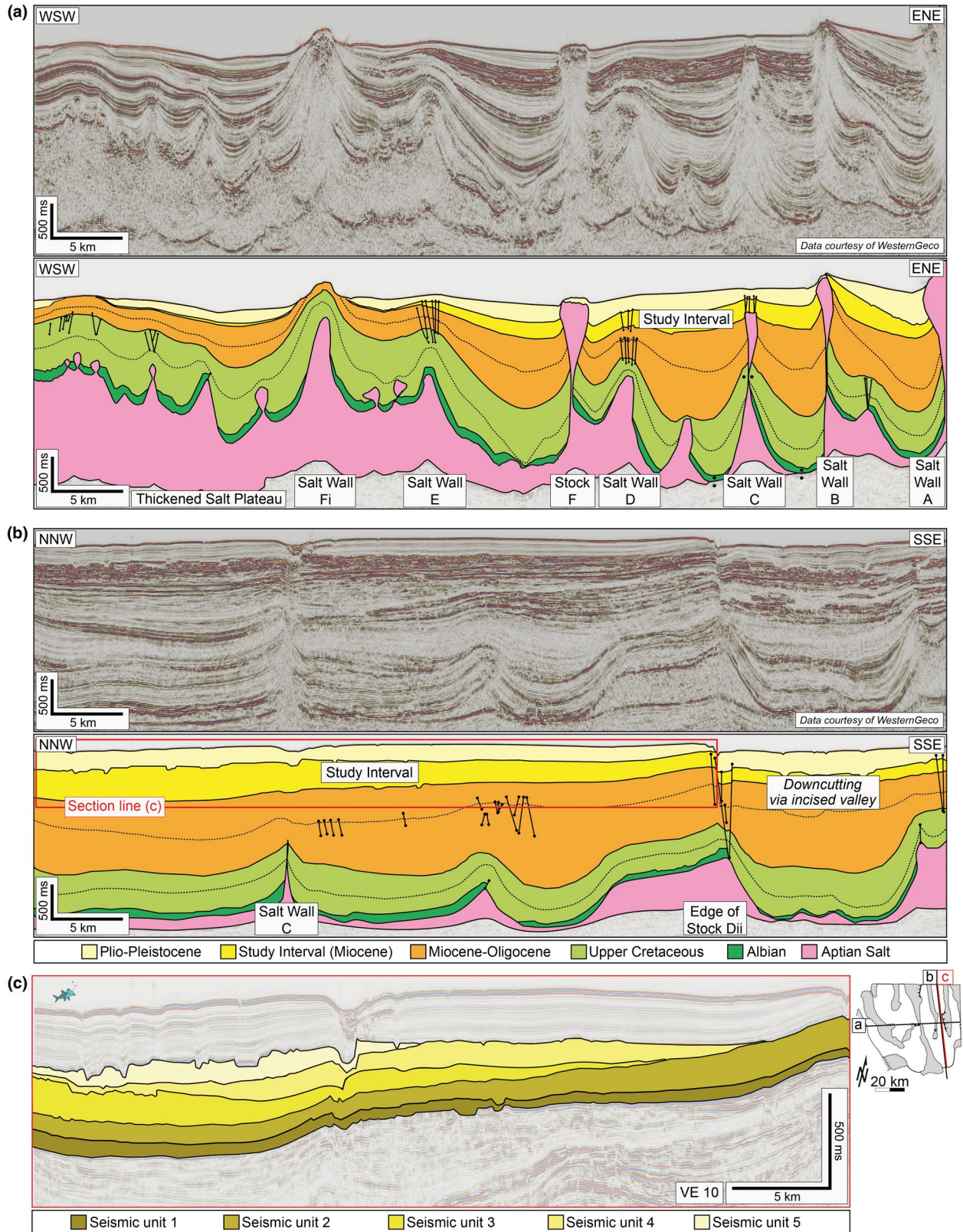
**FIGURE 3** (a) Oblique 3D perspective view of the topography along the present-day sea-floor with corresponding seismic cross-sections shown in Figure 4. Dominant salt-cored structures are outlined in white. The study area can be divided into the eastern domain (elongated co-linear salt walls and minibasins), western domain (segmented and isolated salt-cored structures) and thickened salt plateau. Note how pockmarks (circular negative relief) are largely restricted to the eastern domain and are commonly up-flank of salt walls, surrounding salt stocks or following high sinuosity stacked Miocene turbidite channels. The trimmed pseudo outcrop relief seismic cross-section displays post-salt minibasin infill. MB = minibasin; SW = salt wall; i, ii, iii represent separate segments of a minibasin or salt-cored structure. (b) Oblique 3D perspective view of the top salt draped with the relative thickness of salt within the study area, juxtaposed with a pseudo outcrop relief seismic cross-section displaying top and base salt. VE (vertical exaggeration) = 3

is generally good to excellent within the post-salt stratigraphy. The average frequency in the interval of interest is about 45 Hz, resulting in a maximum vertical resolution of 10–14 m assuming the vertical resolution is a quarter of the wavelength (Brown, 1991) and using an average seismic velocity between 1800 and 2500  $\text{ms}^{-1}$ . The Miocene interval of interest is the shallowest and best-imaged stratal interval with abundant submarine channel-lobe systems. The workflow for our study entailed: (i) defining a seismic stratigraphic framework and mapping bounding horizons, (ii) using time-thickness maps of the seismic units to constrain structural growth, subsidence and sedimentary system development, and (iii) utilising a variety of seismic attribute maps and cross-sectional seismic facies to characterise the deep-water deposits and their evolution.

The seismic stratigraphic framework is based on identification of key seismic surfaces defined by stratal terminations and significant variations in seismic facies and time-thickness distributions (Figures 2 and 4c; Table 1). Horizon stacks containing a number of surfaces for a defined interval are created within Paleoscan™ as preliminary inputs for the stratigraphic

framework and are edited due to the semi-isolated nature of the minibasins. Six horizons are used to define the interval of interest and these form the bounding surfaces of main five seismic units (SU1-SU5; Table 1).

Time-thickness variations within the seismic units are used as proxies for subsidence (primarily within minibasins) and uplift (primarily associated with the growth of salt-cored structures), as well as to identify depositionally driven sediment accumulation fairways (Figure 5). The thicknesses of units along salt flanks is treated cautiously due to the reduced data quality in these areas. We have verified these stratigraphic thickness changes with cross-sectional geometries to validate lateral mapping of deep-water systems in the absence of well data. We have also been conservative in estimating the widths of diapirs given that well data show that salt bodies may be wider than the ‘chaotic’ reflectors used for salt mapping (Jackson & Lewis, 2012; Jones & Davison, 2014). As the study is in the time domain, some geometric distortion is also expected along the salt flanks, but this has limited impact on the results of this study of deep-water depositional systems.



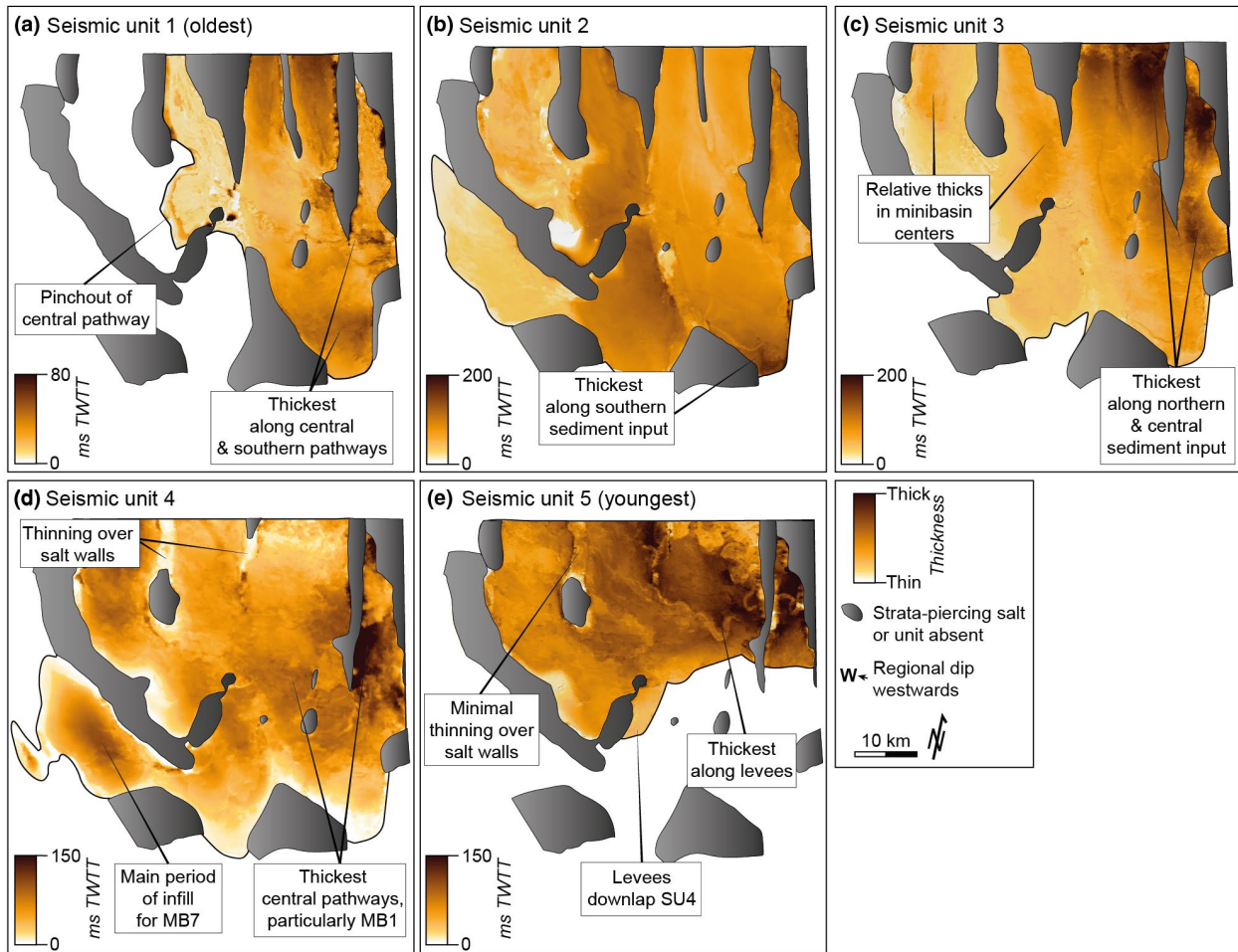
**FIGURE 4** Representative seismic sections with interpretations across the study area displaying the structural and stratigraphic framework for the study (see Figure 3 for cross-section locations). (a) Uninterpreted and interpreted seismic cross-section perpendicular to structural strike illustrating the structural style and variability across the minibasins within the study area. (b) Uninterpreted and interpreted seismic cross-section parallel to structural strike outlining the stratigraphic interval of interest. (c) (Left) Inset of interpreted seismic cross-section from (b) to highlight the thickness variations between the five seismic units within the study interval. (Right) Simplified map of main salt structures outlined in Figure 3

**TABLE 1** Characteristics of bounding horizons for each seismic unit and internal reflector geometries

Seismic unit (SU)	Bounding horizons	Horizon characteristics	Reflector geometries
Youngest	F	Series of down-lapping high-amplitude peaks separating from above low-amplitude Plio-Pleistocene above	
SU5			Continuous high-amplitude reflectors across northern minibasins, conformable with underlying salt-cored highs. Down-laps onto SU4
	E	Regionally continuous high-amplitude trough. Not a major bounding horizon but marks a gradual facies transition from underlying unit	
SU4			Continuous low- and medium-amplitude reflectors with limited on-lapping to underlying salt-cored highs. Eroded by SU5 in parts of MB1, MB2i. On-laps onto SU2
	D	Regionally continuous distinct high-amplitude peak separating from dipping reflectors in the unit below	
SU3			Largely low-amplitude reflectors, down-laps onto SU2
	C	Regionally continuous distinct high-amplitude peak (-trough set) with downlapping reflectors in north	
SU2			Continuous medium-amplitude conformable (to horizon B) reflectors
Oldest	B	Distinct high-amplitude trough (-peak set). Does not continue across all minibasins	
SU1			Continuous low-amplitude conformable (to horizon A) reflectors on-lapping major salt walls/ confined to up-dip minibasins
	A	Distinct high-amplitude trough (-peak set) separating from low-amplitude reflectors below. Does not continue across all minibasins	

Seismic attribute volumes, including spectral decomposition Red-Green-Blue (RGB) colour blends, are generated from the 3D seismic volume and used for the seismic geomorphological analysis of the deep-water deposits. Spectral decomposition transforms the seismic reflection data into the frequency domain, which results in a variety of frequency volumes (Othman, Fathy, & Maher, 2016). In RGB colour blended maps, each colour corresponds to a specific frequency bin that is selected to image channel-lobe systems and mass-transport complexes (MTCs) within the target interval. RGB colour blend maps do not simply display lithology changes, but are also used to outline subtle bed thickness changes, structural edges and fluid varieties. Drastic variations in fluid (and gas) saturation within the Miocene deposits has the potential to boost amplitudes within sand-rich lobes and channels on attribute maps, thereby making

the deposits more pronounced and visible than similar deposits in older, deeper stratigraphy (Maestrelli, Iacopini, Jihad, Bond, & Bonini, 2017). Although time windows around horizons can be defined for these attribute maps, their vertical resolution depends on the 'vertical smearing' during the frequency decomposition. For this study, the Constant Q method is used for frequency decomposition as quality of imaging representative of a seismic unit takes precedence over high vertical resolution (McArdle & Ackers, 2012). To aid calibration and interpretation of planform amplitude or frequency variations observed on attribute maps, cross-sectional seismic facies are closely integrated with planform seismic geomorphology. Different elements of deep-water systems, such as submarine channels, lobes, MTCs and slope deposits have distinctive seismic facies that are defined by differences in their reflection geometry, amplitude, continuity



**FIGURE 5** Time-thickness maps for the seismic units outlining the spatial evolution of the unit thickness within (a) SU1 (oldest unit), (b) SU2, (c) SU3, (d) SU4, and (e) SU5 (youngest unit). See text for detailed descriptions

and conformity (discussed in detail in *Seismic Facies and Depositional Environments*; Table 2).

## 4 | PRESENT-DAY STRUCTURAL CONFIGURATION

The study area contains eight minibasins, each up to 21 km long and 6 km wide, separated by a series of salt-cored highs (Figure 3). Most of the salt-cored highs can be observed on the modern sea-floor where they exhibit c. 85 to 450 ms TWTT of positive sea-floor relief. The planform length and cross-sectional geometry of these salt-cored highs vary spatially across the study area. Salt stock geometry ranges from structures characterised by a relatively thin (c. 3 km diameter) basal pedestal, a very thin or welded stem (secondary weld; sensu Wagner & Jackson, 2011), and a bulbous, teardrop-shaped head (e.g. Stock F; Figure 4a), to those defined by a broader, more pyramidal-shape (e.g. Stock Dii; Figure 4b). Salt walls are typically >30 km long, either dominantly piercing >2.5 s TWTT of the overlying stratigraphy (e.g. Salt Walls A, B; Figure 4a) or dominantly more subdued and

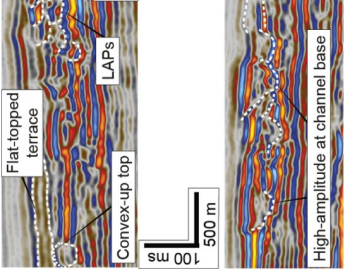


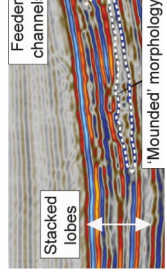

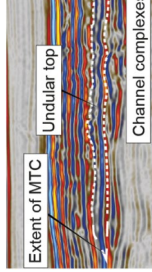

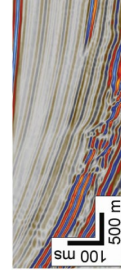
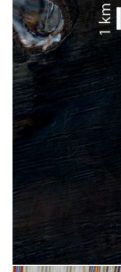
broadly concordant with overlying stratigraphy, appearing as ‘salt pillows’ in many areas (e.g. Salt Walls D, E; Figure 4a). Based on the spatial distribution, continuity and geometry of the salt-cored highs and corresponding minibasins, the structural style of the study area can be divided into two main domains: an eastern domain defined by linear and sub-parallel salt walls and elongated minibasins, and a western domain defined by variably orientated segmented and isolated salt walls, which gradually transition into a down-dip thickened salt plateau.

### 4.1 | Eastern domain

The main structural elements in the eastern domain are four salt walls (Salt Walls A, B, C and D; Figures 3 and 4), and three intervening minibasins (MB1, MB2i, MB2ii and MB3; Figure 3). The minibasins are NNW-trending and elongate (lengths c. 34 km, 5:1 length:width), with MB2ii being a southward extension of MB2i with a more circular planform geometry (length c. 18 km, 1.5:1 length:width). Deeper strata within some minibasins display a W-shaped cross-sectional



**TABLE 2** Dominant seismic facies within the Miocene as observed in cross-section and on seismic attribute (spectral decomposition-*RGB blend*) maps

Seismic facies	Reflection geometry	Depositional environment	Seismic cross-section	RGB blend map
<b>Reflection character</b>				
<b>Submarine channels</b>	V-shaped channel form with distinct basal surface. Top surface varies from horizontal to convex-up. Up to c. 50 ms TWTT thick, width c. 0.25 km, >50 km length	Erosionally-confined stacked channel belts with alternating dominating lithologies, sand or mud fill		
<b>Channel fill – simple</b>	Semi-parallel low- or high-amplitude reflections			
<b>Channel fill – complex</b>	U-shaped channel form, shingled reflections, often overlain by parallel reflections. Up to c. 100 ms TWTT thick, width c. 1 km, >50 km length	Sinuoso meandering and levee-confined stacked channel belts with variable composition; includes lateral accretion packages (LAPs) from channel migration		
<b>Levees</b>	Gull wing to wedge-shaped taper forms, thinning away from channel fills	Overbank deposits from turbidity currents within channels, often fine-grained but can be sand-rich; includes flat-topped terraces		
<b>Lobes</b>	Tabular to mounded morphology, down-laps or amplitude change near edges	Deposits of unconfined flows at channel mouths, mostly sand-rich; includes channelised terminal lobes and unchannelised crevasse splays		
<b>Mass Transport Complexes</b>	Erosive basal surface, undular top surface, some internal thrusts and mounds	Deposits of gravity driven mass wasting from local topographic highs, variable composition		
<b>Background/Hemipelagics</b>	Continuous and parallel (concordant with below deposits), minor normal faulting	Background fine-grained sedimentation in low energy environments or mud-rich turbidity currents		

geometry due to the presence of salt pillows within the minibasin centres, whereas shallower strata have a U-shaped geometry (e.g. between Salt Wall C and D; Figure 4a).

The elongate linear and sub-parallel NNW-trending salt walls separate minibasins, approximately parallel to the shelf break (e.g. between Salt Walls B, C and D; Figure 4a). The salt wall structural style transitions from Plio-Pleistocene piercing salt walls up-dip (e.g. Salt Walls A and B; Figure 4a), to subdued salt-cored highs with concordant overlying stratigraphy down-dip (Salt Walls C and D; Figure 4a). The sea-floor relief for the subdued salt-cored highs is relatively small (up to 110 ms TWTT) compared to the large relief (up to 450 ms TWTT) exhibited by the piercing salt-cored highs (Figure 3). The cross-sectional geometry of salt stocks varies, generally appearing as detached salt bulbs underlain by sub-vertical, (apparent) secondary welds (Stocks Ci and Cii; Figure 4a), or as more pyramidal-shaped salt bodies lacking underlying welds (Stock Di; Figure 3).

## 4.2 | Western domain

The main structural elements in the western domain are two salt walls (Salt Walls E and F; Figure 3) that gradually transition into a thickened salt plateau down-dip. There are four prominent minibasins in this domain (MB4, MB5, MB6 and MB7; Figure 3), with relatively circular planform geometries compared to the eastern domain (c. 21 km length, 2.4:1 length:width). Post-salt thicknesses are similar to the eastern domain (c. 2.4 s TWTT), but the Miocene succession pinches out westwards onto the thickened salt plateau (Figure 4a).

The western domain contains more segmented and isolated salt-cored structures compared to the elongated co-linear salt walls defining the eastern domain. Similar to the up-dip salt walls, Salt Wall E is NNW-trending. Salt Wall F contains a series of distinct segments exhibiting high topographic relief on the sea-floor with variable NE- and NW-trends (Fi, Fii and Fiii; Figure 3). The eastern edge of the thickened salt plateau trends NW, parallel to Salt Wall Fi (Figure 3). The salt plateau has a minimum areal extent of 1,230 km<sup>2</sup> (excluding the attached Stock G), extending westwards beyond the study area. It is consistently thick (c. 1.25 s TWTT), with a rugose top surface due to the presence of small (up to 1.6 km wide and 500 ms TWTT deep) minibasins (Figures 3 and 4).

## 5 | SEISMIC FACIES AND DEPOSITIONAL ELEMENTS

Comparison of the seismic facies with previous studies of deep-water systems aided our identification of depositional elements and interpretation of sedimentary processes in the absence of well-based and lithological calibration within the

study area (e.g. Abreu, Sullivan, Pirmez, & Mohrig, 2003; Deptuck, Steffens, Barton, & Pirmez, 2003; Hansen, Janocko, Kane, & Kneller, 2017; Janocko, Nemec, Henriksen, & Warcho, 2013; Oluboyo et al., 2014; Posamentier & Kolla, 2003). We define five dominant seismic facies based on integration of cross-sections and seismic attribute maps, referring to these as deep-water depositional elements as: (a) channels, (b) levees, (c) lobes, (d) MTCs, and (e) hemipelagics/background deposits (Table 2).

### 5.1 | Submarine channel

This seismic facies contains distinct characteristics, such as planform sinuosity and cross-sectional V- and U-shaped confinement of stacked, somewhat-chaotic medium- to high-amplitude reflections (Table 2). Individual V- and U-shaped deposits are c. 0.25 km wide and c. 20 ms TWTT thick, whereas stacked packages range from c. 0.25 km wide and c. 50 ms TWTT thick for V-shaped geometries, and c. 1 km wide and >100 ms TWTT thick for U-shaped geometries. Deposits may extend in planform for over 50 km. The base of these deposits may contain offlapping shingled reflections dipping towards the youngest deposit or a single continuous high-amplitude reflection if the deposit geometry is below seismic tuning thickness (<10–14 m). Capping reflectors draping the U-shaped bodies may be ‘convex-up’ (positive-relief) or flat. In planform, the V-shaped bodies tend to have lower sinuosities (near 1) than the U-shaped bodies (>1.5).

Similar seismic facies and seismic geomorphology have been observed in many other studies of deep-water depositional systems (e.g. Deptuck, Sylvester, Pirmez, & O’byrne, 2007; Gee & Gawthorpe, 2006; Hadler-Jacobsen et al., 2005; Hansen et al., 2017; Janocko et al., 2013; Niyazi et al., 2018; Oluboyo et al., 2014; Pirmez, Hiscou, & Kronen, 1997; Posamentier & Kolla, 2003; Prather et al., 1998) and following these works, they are interpreted as submarine channel deposits. We will abide to the sedimentological terminology of channel belts and channel complexes, the latter referring to vertically stacked multi-story channel belts with varying offset (Collinson & Thompson, 1982). Channel complexes in this study are interpreted to contain both sand-rich and mud-rich channel fills based on cross-sectional geometry and amplitude contrasts on seismic attribute maps. High-amplitude channel fills, inferred to be sand-rich, contain positive-relief due to differential compaction, whereas low-amplitude channel fills, inferred to be mud-rich, have flat capping reflections if the channel form is >30 ms TWTT thick (Posamentier, 2003). Channel complexes are observed to be dominantly erosional, meandering or leveed (Janocko et al., 2013). Erosionally based complexes are defined by lower sinuosities and V-shaped channel forms, whereas meandering systems have higher sinuosities with lateral

accretion packages (LAPs), and relatively wide, U-shaped channel forms. Leveed systems often contain U-shaped channel forms encased by high- or low-amplitude wedge-shaped geometries. Hybrids of these channel complex varieties are also common in the study area, such as wide meander belts (i.e. lateral extent of the channel meanders) adjacent to low-amplitude levees or terraces (see below).

## 5.2 | Levees

In cross-section, this seismic facies is characterised by two or more reflections that have a gull-wing-shaped geometry and are located directly adjacent to submarine channels (Table 2). This seismic facies is up to 80 ms TWTT thick, and thins away from the channel axis over horizontal distances of up to 12 km. Reflections vary in amplitude, typically decreasing away from the channel axis before downlapping onto underlying deposits.

The geometry and reflection characteristics of this seismic facies has been recognised by other authors as external levees associated with channel complexes, formed when the height of turbidity currents exceeds the confinement of the channel form and spill sediment onto the areas surrounding the channel axis (e.g. Deptuck et al., 2007; Janocko et al., 2013; Oluboyo et al., 2014; Posamentier & Kolla, 2003). Often this overspill is fine-grained due to flow stripping, resulting in a mud-dominated deposit and the low-amplitude response commonly observed in seismic reflection data (Table 2).

## 5.3 | Lobes

This seismic facies is composed of distinctive, sub-parallel continuous medium- to high-amplitude reflections that are tabular to lenticular in cross-section. It has a maximum thickness of 50 ms TWTT, typically thinning and downlapping towards the outer edges (Table 2). On seismic attribute maps, these deposits have a distinct tongue-shape and are invariably located down-dip of submarine channels. Individual lobe-shaped deposits generally contain a 'feathery' texture, distinguished by a branching outwards dendritic pattern. The boundaries of these lobes can be denoted by amplitude changes, such as a sudden dimming, although it can be difficult to differentiate individual lobes within the larger and thicker deposit. Individual lobes are typically 4–5 km long and 1–2 km wide, whereas the larger deposit conforms to the shape of the minibasin accommodation it is infilling, with average lengths 8–18 km and widths 8–20 km.

These lobe-shaped deposits have been observed along the slope through to basin-floor, in both ponded and unconfined deep-water settings (Doughty-Jones et al., 2017; Gamberi & Rovere, 2011; Hay, 2012; Posamentier & Kolla, 2003), and

they are variably referred to as channelised lobes, frontal splays, sheet sands and submarine fans. We use the Pr elat, Covault, Hodgson, Fildani, and Flint (2010) hierarchical terminology and refer to the larger deposits as *lobe complexes* comprised of *lobes*, with the internal distributary channels forming dendritic patterns. Taking into consideration tuning thickness effects on the seismic attribute maps, it is possible to differentiate the lobe axis and the outer lobe fringe given the amplitude contrasts may at least partly reflect the spatial distribution of mudstone and sandstone (e.g. Figure 9a and Figure 13; Doughty-Jones et al., 2017).

## 5.4 | Mass-transport complexes

This seismic facies occurs adjacent to salt-cored highs and consists of low- to moderate-amplitude reflections with a discontinuous and chaotic character forming bodies up to 50 ms TWTT thick and 15 km wide (Table 2). Internally these bodies may contain dipping reflections (internal thrusts) that strike parallel to the edges of nearby topography. The base of these deposits is sharp and often truncates underlying reflections, whereas the top surface is generally irregular and undulatory. In planform, these deposits may blend in with surrounding background deposits, but have a speckled appearance.

This distinctly chaotic seismic facies is interpreted as deposits of mass-wasting, so called MTCs (Doughty-Jones, Lonergan, Mayall, & Dee, 2019; Olafiranye, Jackson, & Hodgson, 2013; Ortiz-Karpf et al., 2015; Posamentier & Kolla, 2003; Wu, Jackson, Johnson, Hodgson, & Nugraha, 2020). Such mass-wasting processes can be erosive, leading to scouring of the underlying strata on a seismic-scale (Bull, Cartwright, & Huuse, 2009). Due to the location of these deposits adjacent to salt-cored highs and presence of syn-depositional thrusts, we interpret most of these deposits as locally sourced MTCs derived from the flanks of surrounding topographic highs (Martinez, Cartwright, & Hall, 2005). The speckled appearance observed on seismic attribute maps may be due to these internal thrusts or megaclasts incorporated in the deposit (Ortiz-Karpf, Hodgson, Jackson, & Mccaffrey, 2017).

## 5.5 | Hemipelagics/background deposits

The characteristic signature of this seismic facies is low- to moderate-amplitude reflections, that are parallel and conformable to underlying deposits (Table 2). These deposits range from a few reflections up to hundreds of milliseconds TWTT in thickness, and are typically continuous across minibasins for tens of kilometres.

Similar seismic facies have been observed in many areas, and are believed to be the deposition of pelagic and

hemipelagic mud and silt during sediment starvation in low-energy environments (Hadler-Jacobsen et al., 2007; Oluboyo et al., 2014). It should also be noted that not all of these deposits are from suspension settling; some may be fine-grained, low-density turbidity currents (Boulestex et al., 2019; Straub & Mohrig, 2009).

## 6 | TECTONO-STRATIGRAPHIC EVOLUTION

The seismic stratigraphic framework for the study interval is based on six key seismic horizons that sub-divide the Miocene interval of interest into five seismic units (Table 1). The following sections will describe time-thickness variations (Figure 5) and outline the main sediment transport pathways using representative seismic attribute maps for each unit (Figures 6, 7, 9, 11 and 14; see Table 3 for summary).

### 6.1 | Seismic unit 1

#### 6.1.1 | Summary of observations

Seismic Unit 1 (SU1) is the oldest seismic unit in the study and is dominated by background deposits contained within the up-dip minibasins (MB1, MB2i, MB2ii, MB3 and MB4) by salt walls (Figure 6; Table 3). SU1 thickness is relatively constant, c. 40 ms TWTT, throughout the majority of the minibasins. Subtle thicks occur at the sediment entry points in MB2ii, the southern portion of MB1 and northern portions of MB2i and MB3 (c. 60 ms TWTT; Figure 5a). SU1 is thinnest in MB4 where the unit extends from the up-dip MB3 through a segment boundary, defined here as <2 km topographic lows developed between co-linear folds, along Salt Wall D (Figure 6).

#### 6.1.2 | Depositional elements

Based on the volume windows provided by a series of attribute maps, SU1 is comprised of 36% background deposits, 34% poorly imaged lobes and 30% channel complexes. The channel complexes can be further classified as 53% lacking observable LAPs and 47% containing well-developed LAPs. Some of the lobe deposits are difficult-to-resolve on attribute maps and the start of these deposits are inferred where trunk channels branch outwards before terminating. SU1 is comprised of two main sediment transport pathways, Pathways A and B, both of which enter the study area in the east at an orientation transverse-to-structure (Figure 6). The northern pathway, Pathway A, consists of multiple sinuous channel complexes that are strongly influenced by salt-cored

structures, whereas the southern pathway, Pathway B, is composed of lobes confined within MB2ii.

### 6.1.3 | Pathway A

The channel complexes within Pathway A enter MB1 perpendicular to structural strike, between Salt Wall A and Stock A (Figure 6). The northern channel complex ( $A_N$ ) contains low sinuosity (average 1.06) channels diverted northwards to trend parallel to Salt Wall B, whereas the main high sinuosity (average 1.64) channel complex crosses the southern end of Salt Wall B into MB2i, and then passes between Stocks Ci and Cii into MB3. Older channel complexes along Pathway A are diverted north of these salt stocks and across Salt Wall C, where the system deposits a series of lobes in MB3 with dimensions c. 4 km by 2 km (Figure 6). The sinuosity of Pathway  $A_N$  channels increases in MB3 (from an average of 1.05 to 1.79) as they are diverted northwest towards a segment boundary along Salt Wall D. Once the channel complex crosses into MB4, the meander belt wavelength increases drastically (from c. 2.5 to 10.8 km) and the system is diverted north to trend parallel to adjacent salt walls before exiting the study area (Figure 6).

The most southern channel complex ( $A_S$ ) within Pathway A enters MB2ii as a series of channel complexes without evident LAPs. A single channel complex feeds several small lobes (average 1.4 km by 2.6 km) to the south of the channel axis before terminating in a few, larger lobes (average 2.0 km by 5.0 km) blocked down-dip by Stock D.

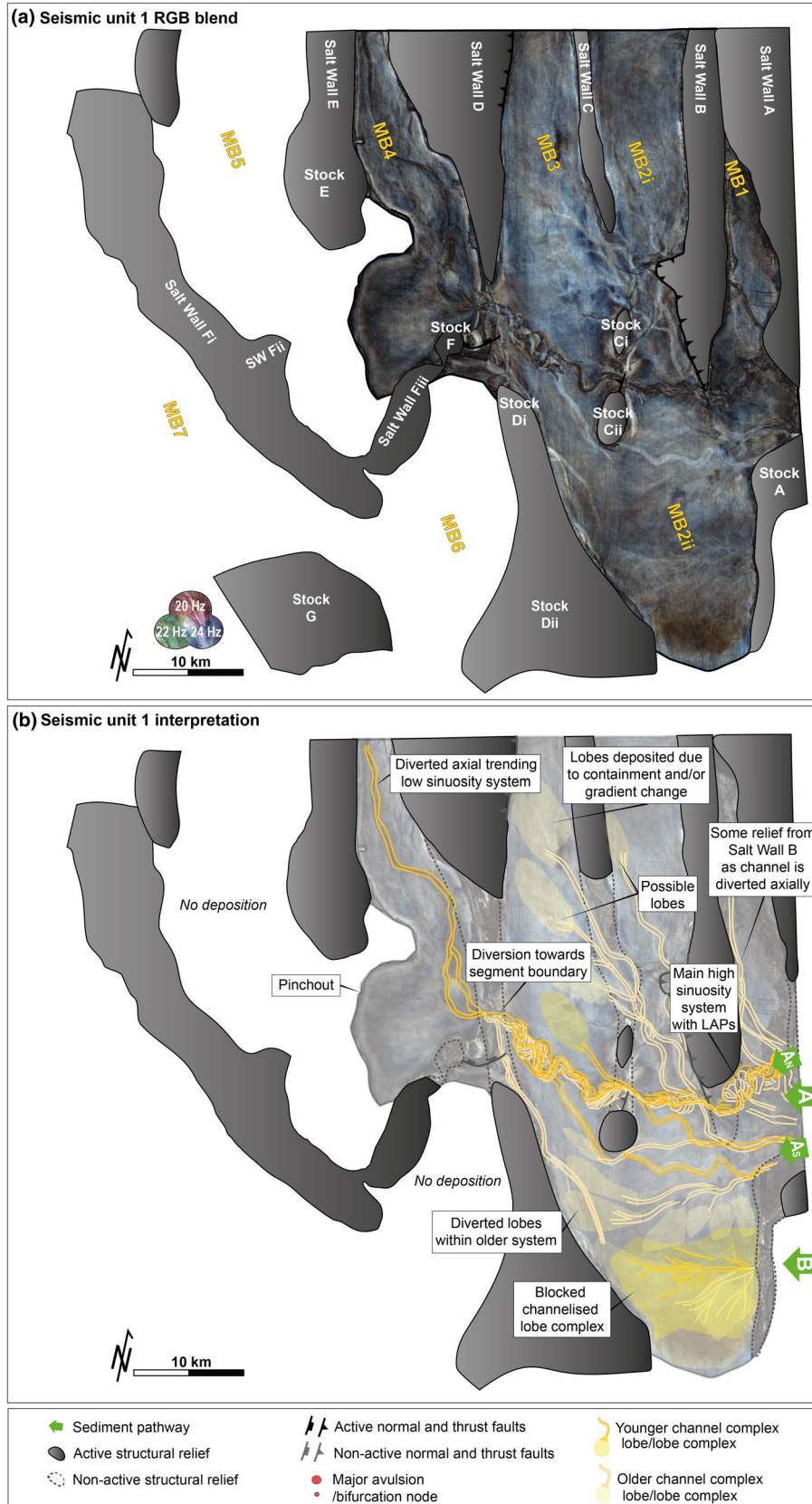
### 6.1.4 | Pathway B

Pathway B lies to the south of Pathway A, in the southeast of the study area and consists of a large lobe complex (c. 6.5 km by 11.8 km) within MB2ii, that is sourced from south of Stock A (Figure 6). Individual lobes are inferred by subtle changes in distributary channel orientation, and although some distributary channels are diverted north parallel to Salt Wall D, the lobe complex is largely blocked by Stock D and confined within MB2ii.

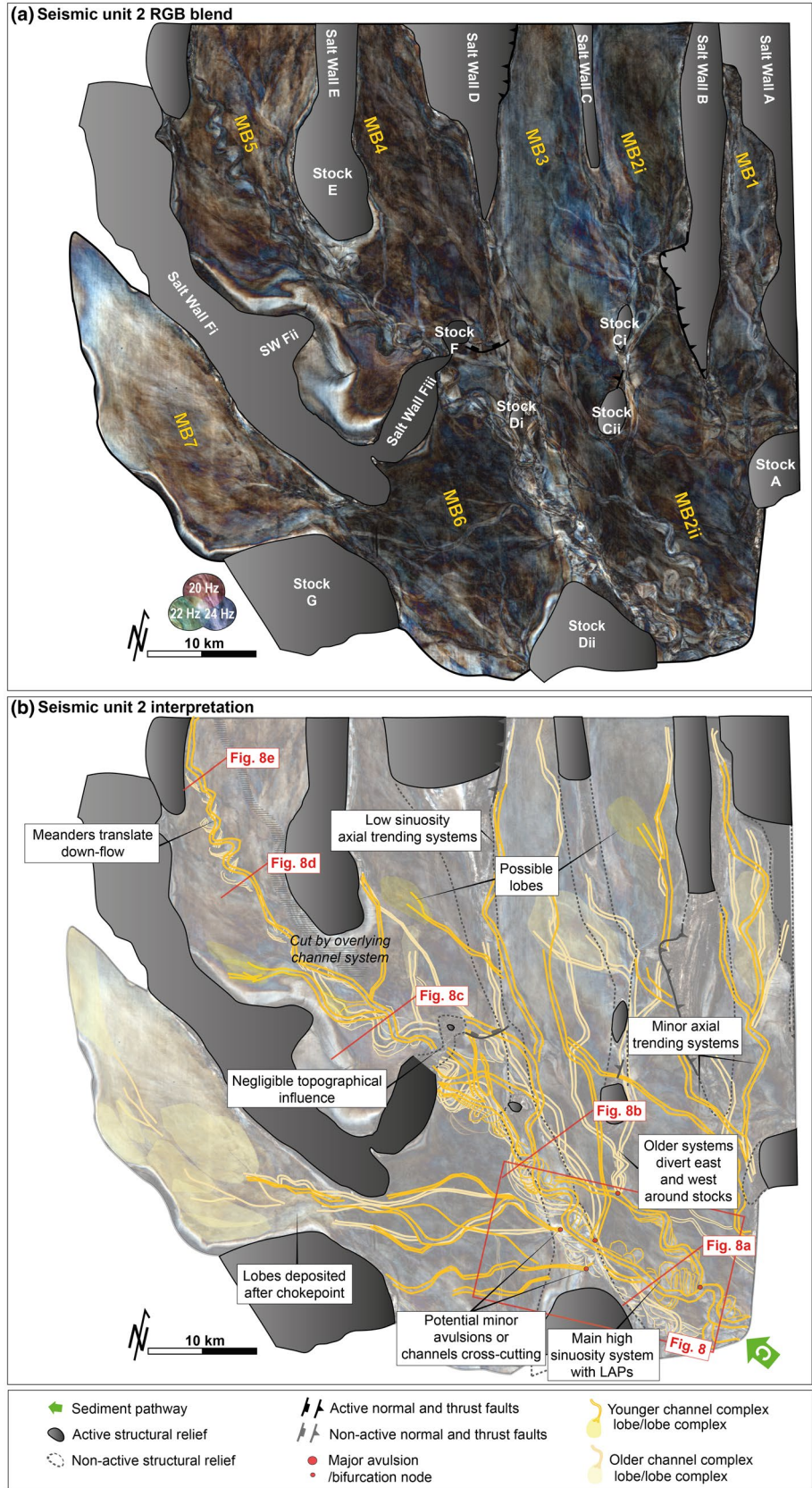
## 6.2 | Seismic unit 2

### 6.2.1 | Summary of observations

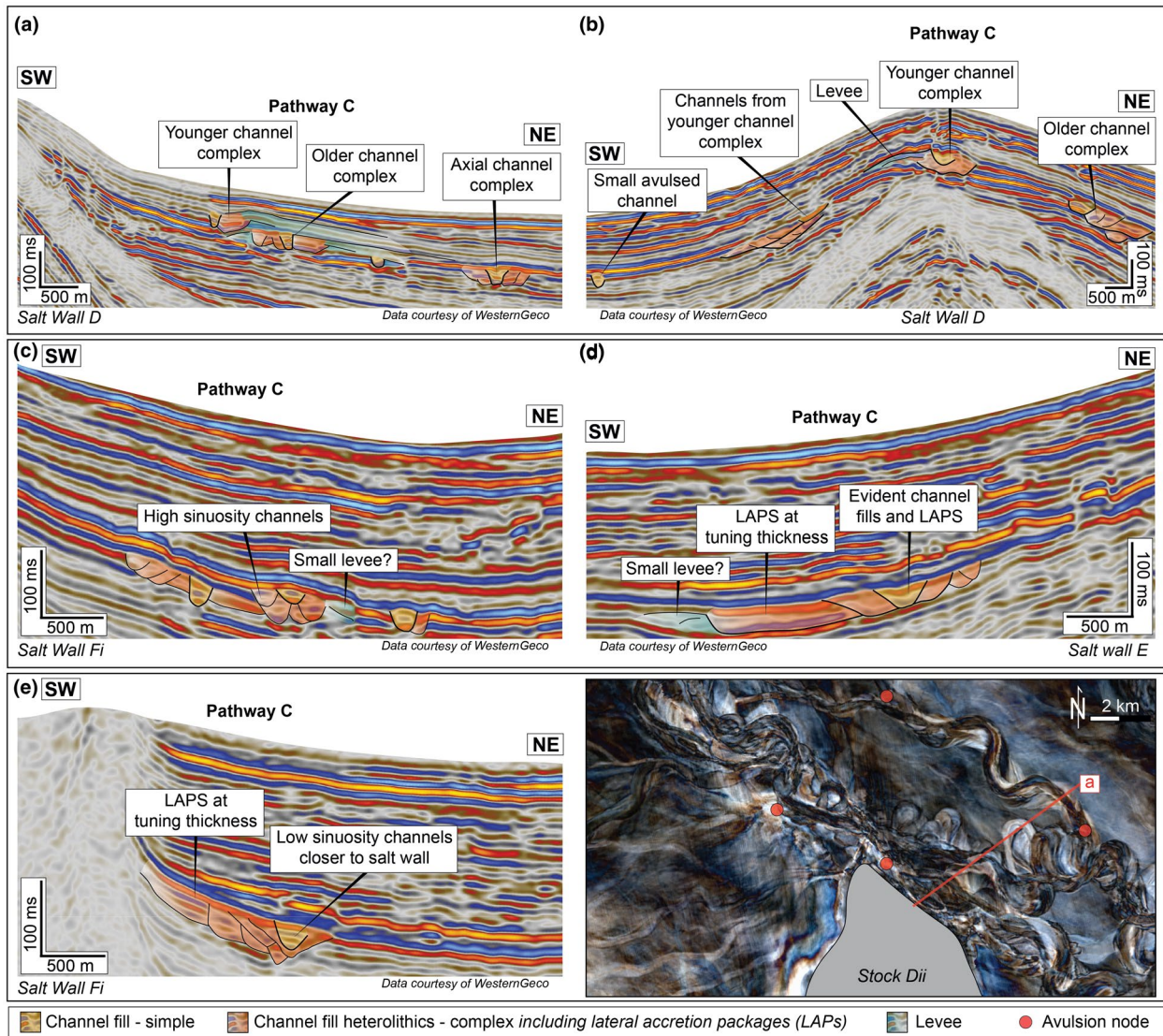
Seismic Unit 2 (SU2) is more extensive than SU1, extending into down-dip minibasins, as well as having different sediment input directions and locations (Figure 7; Table 3). The isochron thicks for SU2 are pronounced along the main sediment transport pathways reaching up to 200 ms



**FIGURE 6** Representative seismic geomorphology for the oldest unit, SU1. (a) Representative spectral decomposition attribute map for SU1 with main salt-cored structures and minibasins labelled. (b) Simplified map of the main submarine channels and lobes for SU1. Older systems are lighter colours, while younger systems are darker colours. Active/positive topographic relief of the salt structures is displayed in solid grey and the inactive/negligible topographic relief is outlined with dashed lines. The major sediment input pathways (A and B) are marked with green arrows. See text for a detailed description of the unit's evolution



**FIGURE 7** Representative seismic geomorphology for SU2. (a) Representative spectral decomposition attribute map for SU2 with main salt-cored structures and minibasins labelled. (b) Simplified map of the main submarine channels and lobes for SU2. Older systems are lighter colours, while younger systems are darker colours. Active/positive topographic relief of the salt structures is displayed in solid grey and the inactive/negligible topographic relief is outlined with dashed lines. The major sediment input pathway (C) is marked with a green arrow. See text for a detailed description of the unit's evolution



**FIGURE 8** Seismic cross-sections highlighting Pathway C in SU2 (see Figure 7 for positions on map). (a) Near sediment input entry point, (b) crossing over Salt Wall D where there are potentially numerous minor avulsions westwards of small channel complexes, (c) down-dip of Salt Wall Fiii and Stock F, (d) through high sinuosity and relatively undisturbed channels in MB5, and (e) through low sinuosity channels with no levees closer to Salt Wall Fi. (Right) The attribute map displays the high sinuosity channels entering the study area and the location of avulsion nodes on the outer meander bends. Small channel complexes are avulsed northwards and westwards

TWTT, most notably within MB2ii (Figure 5b). Additional isochron thicks occur within MB4 and MB6 (c. 130 ms TWTT), before the unit thins down-dip into MB5 and MB7 (c. 45 ms TWTT).

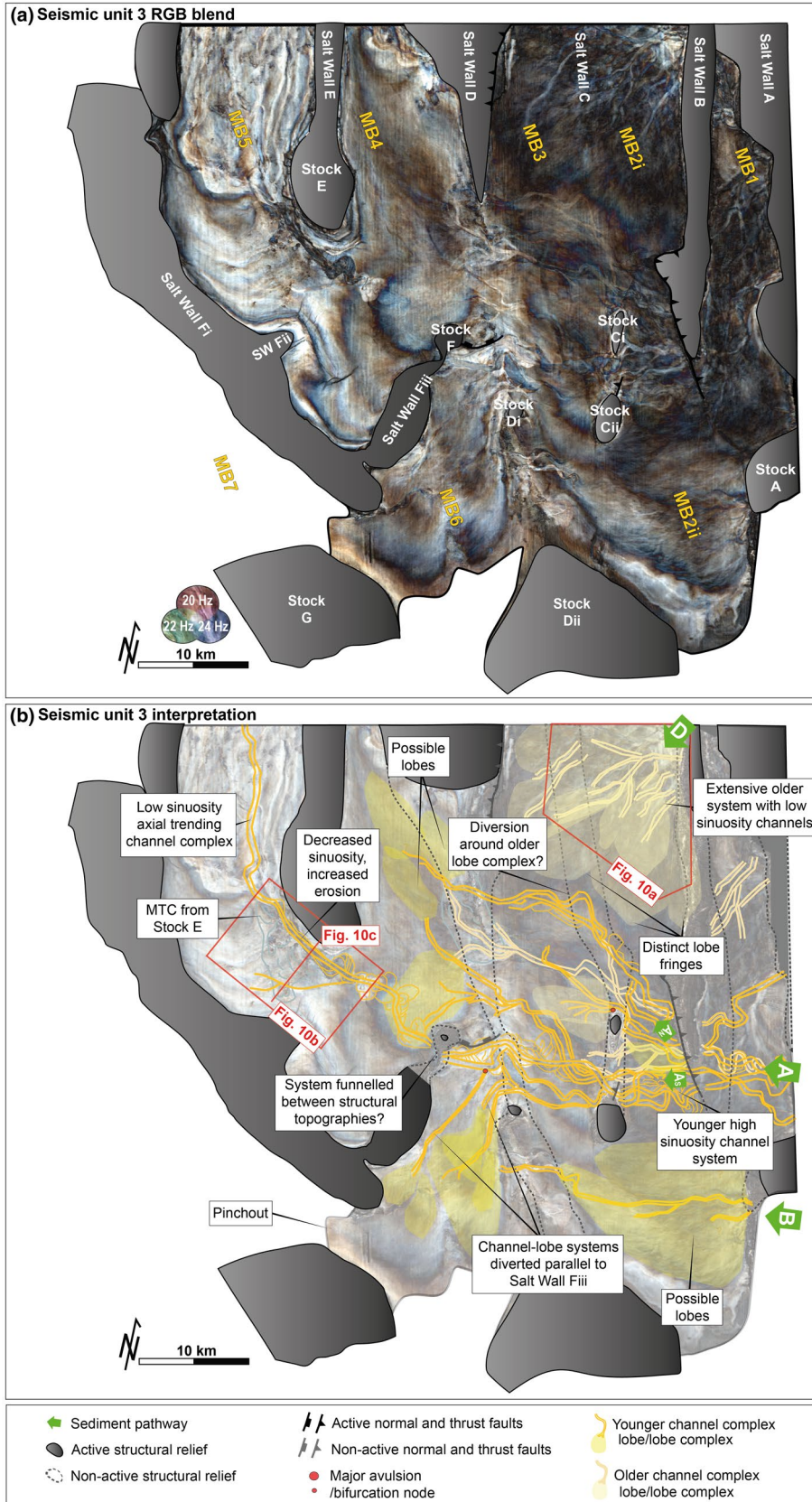
### 6.2.2 | Depositional elements

The seismic facies for this seismic unit is 47% dominated by extensive channel complexes, with 38% background deposits and 15% lobes. The channel complexes can be sub-divided into 51% lacking observable LAPS and 49% containing LAPS. As with SU1, the lobes are difficult to resolve and often inferred by the termination of outward-branching

feeder channels. The main sediment routing system for SU2 is Pathway C, which enters from the study area in the south-east corner.

### 6.2.3 | Pathway C

Pathway C is orientated oblique-to-structure and consists mainly of channel complexes trending broadly north-west (Figure 7). There is one main c. 2.5 km wide and c. 80 ms TWTT thick channel complex with LAPS (Figure 8). Sinuosity is highest for the oldest LAPS within MB2ii (average 2.77), and decreases significantly (average 1.08) in the youngest LAPS within MB2ii and MB6. The channels



**FIGURE 9** Representative seismic geomorphology for SU3. (a) Representative spectral decomposition attribute map for SU3 with main salt-cored structures and minibasins labelled. (b) Simplified map of the main submarine channels and lobes for SU3. Older systems are lighter colours, while younger systems are darker colours. Active/positive topographic relief of the salt structures is displayed in solid grey and the inactive/negligible topographic relief is outlined with dashed lines. The major sediment input pathways (A, B and D) are marked with green arrows. See text for a detailed description of the unit's evolution



continue north around the salt-cored relief of Stocks Ci and Cii until the channel width decreases to near seismic resolution, potentially depositing thin lobes further down-dip in MB2i, MB3 and MB4.

Several avulsion nodes occur along the outer meander bends of the main channel belts above Salt Wall D (Figure 8a,b). A series of smaller channel complexes develop from these nodes, directed either northwards into MB3, or westwards into MB6 and onwards towards MB7 (Figure 7). Instead of emanating from minor avulsion nodes, these erosionally based channels could in fact lie at slightly different stratigraphic levels to the main channels, with our RGB blend technique unable to fully distinguish between them. On the western side of MB6 the channel complexes encounter a narrow c. 5 km long 'chokepoint', defined as >2 km elongated narrow passageways between topographic highs, between Salt Wall Fi and Stock G. Here, the channel complexes coalesce into an erosional channel complex that feeds thin axial lobes (c. 30 ms TWTT) within MB7 (Figure 7).

The main channel complex with LAPs continues to the northwest beyond the avulsion nodes, initially containing high sinuosity channels (average 2.12) as it is apparently funnelled between Salt Wall Fiii and Stock F, before spilling into MB4 (Figures 7 and 8c). As the main channel complex passes down-dip from MB4 into MB5, the sinuosity decreases (average 1.10) along the steeper gradient near Stock E, but increases once again (average 1.63) further into MB5. Here the channel meanders translate down-flow in the lower gradient minibasin centre (Figures 7 and 8d). The channel complex contains no levees adjacent to Salt Wall Fi in MB5 and decreases in sinuosity before exiting the study area as an axial system (Figures 7 and 8e).

## 6.3 | Seismic Unit 3

### 6.3.1 | Summary of observations

Seismic Unit 3 (SU3) has different sediment input locations and directions than SU2, with the sediment depocentres shifting from the south of the study area to the north (Figures 5c and 9; Table 3). The isochron thicks for SU3 are dominated by the relatively older sediment Pathway D in the northeast, largely within MB2i (c. 180 ms TWTT; Figure 5c). Relative thicks of up to 85 ms TWTT occur within the down-dip minibasin centres for younger sediment Pathways A and B. Unlike SU2, deposition in SU3 does not continue into MB7.

### 6.3.2 | Depositional elements

SU3 is comprised of 39% lobes, 31% background deposits, 25% channel systems and 5% MTCs. The channel complexes

can be sub-divided in a similar way to SU2 into 65% containing LAPs and 35% lacking observable LAPs. Lobe complexes are 64% highly channelised and 36% are difficult-to-resolve. SU3 can be divided into a lower (older) sub-unit dominated by lobe complexes with low sinuosity trunk channels from Pathway D, and an upper (younger) sub-unit consisting of widespread, high sinuosity, initially transverse-to-structure channel-lobe systems of sediment Pathways A and B (Figure 9).

### 6.3.3 | Pathway D

In the lower (older) sub-unit of SU3, Pathway D forms a substantial (c. 185 km<sup>2</sup> area) sediment routing system and is the only system to enter from the northeast of the study area (Figure 9). Pathway D is composed of numerous lobe complexes which can be sub-divided into three phases based on reflection characteristics and channelisation (Lobes Di, Dii and Diii; Figure 10a). The oldest lobe complex (Di) is composed of parallel low- to medium-amplitude reflections with a few notable down-laps indicating lobe fringes, and only a few observable channels. These extensive lobes are largely confined within MB2i with some spill-over across Salt Wall C into MB3 (Figure 10a). Lobes within Dii comprise of medium- to high-amplitude reflections with numerous low sinuosity (average 1.07), c. 300 m wide trunk channels, which are diverted around Lobe Di topography to deposit lobes further down-flow within MB2i and MB3 (Figure 10a). The youngest lobes (Diii) contain high-amplitude continuous reflections with indistinguishable lobe fringes. These lobes have few trunk channels (c. 200 m wide), but contain numerous distributary channels (c. 20 m wide).

### 6.3.4 | Pathway A

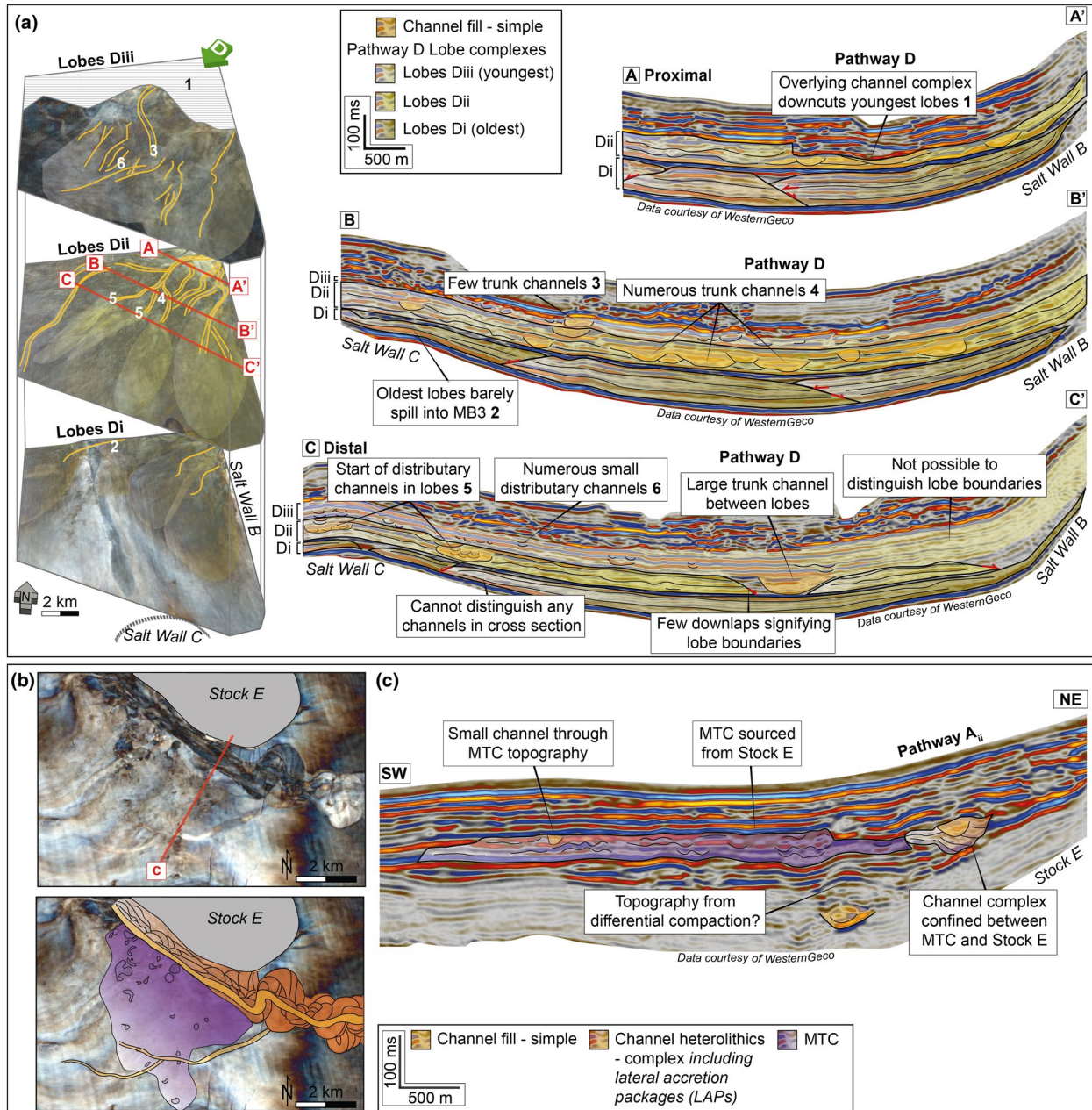
In the upper (younger) sub-unit of SU3, sediment Pathways A and B, return to a transverse-to-structure orientation of sediment routing. Pathway A is composed of a series of main channel complexes along a c. 9 km transect, similar to Pathway A in SU1, but with a greater number of thicker channel complexes (Figure 9). This sediment transport pathway splits into a NW-trending pathway (A<sub>N</sub>) and a W-trending pathway (A<sub>S</sub>; Figure 9). The low sinuosity channels of A<sub>N</sub> (average 1.12) are diverted west of Pathway D and over Salt Wall C down-dip into MB3 (Figure 9). As the channels cross over Salt Wall D into MB4, they either decrease in width to below seismic resolution or they deposit thin, low-amplitude, axial lobes (Figure 9). Pathway A<sub>S</sub> continues transverse-to-structure, confined between Stocks Ci and Cii, across MB2ii towards Salt Wall D. The main channel complex is funnelled between Salt Wall Fiii and Stock F, although some

minor channels deposit a series of lobes south of Salt Wall Fiii (Figure 9). Within the proximal area of MB5 the channel complex is confined between the southern end of Stock E and a c. 18 km<sup>2</sup> detached MTC derived from the flank of the nearby salt stock (Figure 10b,c). The channel complex decreases in sinuosity (average 1.67 to 1.02) and width (c. 1.5 km to 0.5 km) across this corridor and continues axially along MB5 and northward out of the study area (Figure 10b).

A small-avulsed channel is intricately routed through the tortuous MTC topography (Figure 10b).

### 6.3.5 | Pathway B

Pathway B appears similar in extent and geomorphology to the blocked lobe complex within Pathway B of SU1. It also



**FIGURE 10** (a) (Right) Interpreted proximal to distal seismic cross-sections through Pathway D's large SW-trending lobe complex in SU3. The lobe complex is divided into Di, Dii and Diii (oldest to youngest) based on seismic character and channelisation. (Left) Oblique view of the attribute maps for the three lobe complexes displaying shifting lobes and trunk channels. Exaggerated vertical scale. (b) Uninterpreted and interpreted RGB blends from SU3 (see Figure 9 for position on map) outlining the locally derived MTC from Stock E and the corresponding influence on a channel complex (e.g. decreased sinuosity and meander belt width). A small avulsed channel crosses the MTC topography before decreasing below seismic resolution. (c) Interpreted seismic cross-section showing the seismic character of the MTC and a decreasing thickness towards the deposit edges (see (b) or Figure 9 for position on map)



consists of transverse-to-structure input south of Stock A, depositing feathery-edged lobes up-dip of Stock Dii (Figure 9). In addition, the lobes appear to be cut by a younger channel complex that continues westwards across MB2ii.

## 6.4 | Seismic unit 4

### 6.4.1 | Summary of observations

Seismic Unit 4 (SU4) is more extensive than SU3, extending down-dip into MB7 and is dominated by widespread channel-levee systems (Figure 11; Table 3). The time-thickness map for SU4 highlights thicks that largely follow the main sediment transport pathways through the centre of the study area, reaching up to c. 150 ms TWTT near Salt Wall B (Figure 5d). Relative thicks of c. 70 ms TWTT follow stacked channel complexes that continue northwest into MB5, or southwest into MB7, terminating as lobes.

### 6.4.2 | Depositional Elements

SU4 is predominantly composed of 50% channel systems and 41% lobes, with 9% background deposits. The channel complexes dominating the northern section of the study area can be sub-divided into 56% containing LAPs, 32% lacking LAPs and 12% multi-story channel complexes. Three main sediment fairways occur within SU4, Pathways A, B and E, all of which enter the eastern side of the study area at a high angle to structural strike. The main sediment transport pathway is the central Pathway A, which consists of numerous major channel complexes extending down-dip into MB5 and MB7. Pathway B is a lobe complex largely confined to MB2ii, whereas Pathway E is composed of numerous relatively small channel complexes.

### 6.4.3 | Pathway A

Pathway A is an extensive sediment fairway and enters MB1 as a series of channel complexes along a c. 5 km wide section across Salt Wall A and continues down-dip into MB2ii, MB6 and MB7 (Figure 11). This pathway can be divided into a northern channel complex ( $A_N$ ), a central collection of channel complexes ( $A_C$ ), and a long (>43 km) southern channel complex ( $A_S$ ). Collectively, the channel complexes have high sinuosities (average 2.58) and meander belt widths (average 1.7 km) within MB1, values that substantially decrease down-dip of Salt Wall B (Figure 11).

The southern channel complex of Pathway A ( $A_S$ , Figure 11) firstly deposits a lobe complex (Ai) that extends southwest into MB2ii, and is later eroded by an extensive

low sinuosity channel complex. This channel complex is diverted c. 1.6 km south around Stock Cii and locally contains well-developed levees, particularly on its southern side. Channel sinuosity increases immediately down-dip of Salt Wall C (average 1.2 to 1.40), where the channel feeds a series of backstepping lobes (Aii and Aiii) within MB6 (Figure 11). The main channel complex continues westward, diverted c. 3 km south by Salt Wall Fiii, and continues as a narrow, erosive channel through the confining 'chokepoint' between Salt Wall Fi and Stock G (Figure 12a–c). Upon entering MB7 the channel complex transitions through the CLTZ (Figure 12d) into a widespread down-dip terminal lobe complex (Aiv) that is up to 100 ms TWTT thick (Figure 12e). The trunk channels of the lobes are c. 0.3 km wide, whereas the distributary channels are at the limit of seismic resolution and appear as a feathery texture on RGB attribute maps (Figure 11).

The central channel complex of Pathway A ( $A_C$ , Figure 11) crosses Salt Wall B and subsequently decreases in average sinuosity (average 3.20 to 1.46) and meander belt width (average 2.5 to 1.3 km). Within MB3 and MB4 these channels are of high sinuosity (average 2.1), but the youngest channel belt sinuosity decreases (average 1.1) along Stock F. The system deposits a series of lobes along the confining Salt Wall Fi and leaves the study area as axially trending channel complexes.

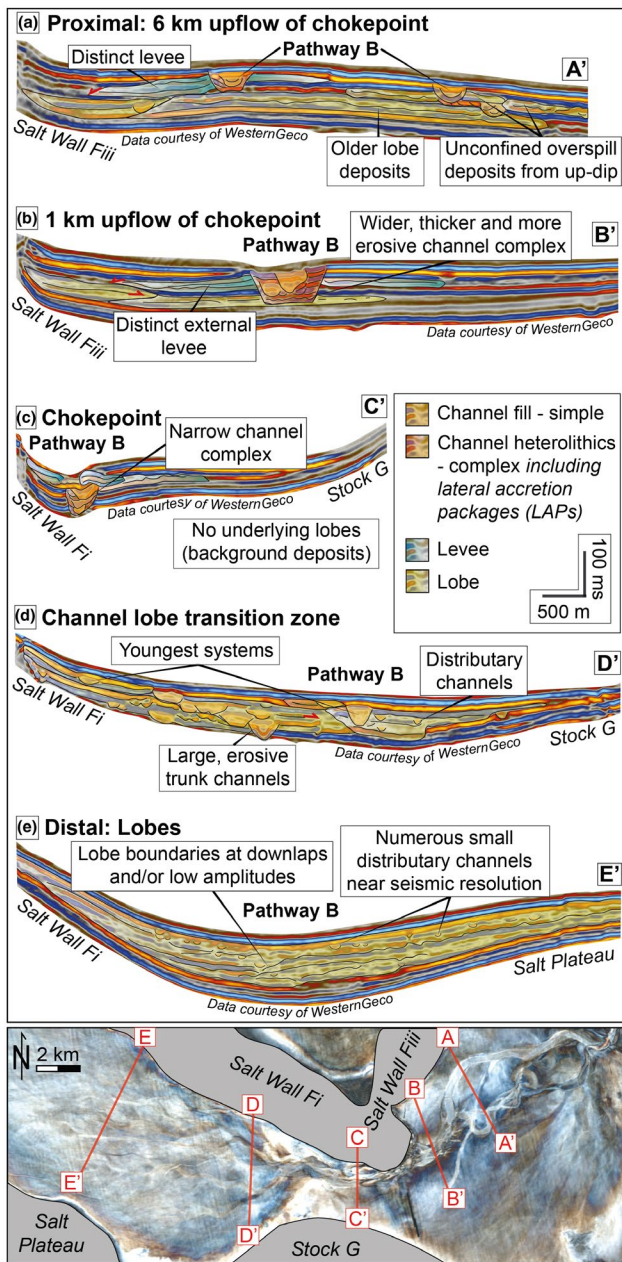
The northern channel complex of Pathway A ( $A_N$ ) is c. 1.2 km wide, up to 85 ms TWTT thick, and is of relatively high sinuosity (average 1.5 in MB3; Figure 11). The channel complex is diverted axially along MB4, where its sinuosity decreases (average 1.5 to 1.2) and it lacks LAPs. An older channel complex along this sediment transport pathway crosses Salt Wall D before being diverted northward down-dip of Salt Wall D and along the centre of MB4 (Figure 13). Sinuosity and meander belt width initially increase into MB4 (average sinuosity 1.06 to 1.55, and width 0.7 to 1.5 km) before finally decreasing when parallel to the salt walls (average sinuosity 1.16, and width 1.1 km).

### 6.4.4 | Pathway B

Pathway B is essentially a continuation of the minor sediment Pathway B developed in SU3, but contains better-defined lobes and a younger high sinuosity (average 1.59) channel complex eroded by Pathway  $A_S$  (Figure 11). The lobes fill MB2ii and are blocked to the southwest by Stock Dii.

### 6.4.5 | Pathway E

Due to down-cutting from a younger channel complex (SU5), it is not possible to document the exact entry point



**FIGURE 12** Interpreted seismic cross-sections displaying changing channel geomorphology (e.g. channel width, erosional depth) along the 'chokepoint' between Salt Wall Fi and Stock G within SU4 (see Figure 11 for position on map). Transitioning from (a) proximal channels, 6 km up-flow of chokepoint, to (b) 1 km upflow of chokepoint, to (c) narrow chokepoint, to (d) channel-lobe transition, and finally to (e) distal downflow lobes

for Pathway E; there may be a single or multiple entry points along a c. 5 km transect on the eastern edge of the study area (Figure 11). Pathway E contains numerous low sinuosity (average 1.07), narrow (c. 0.15 km) channels with rare LAPs. The channels cross MB2i at a high angle to the bounding salt structures.

## 6.5 | Seismic unit 5

### 6.5.1 | Summary of observations

Seismic Unit 5 (SU5) is dominated by stacked, multi-story channel complexes and terminal lobes within the northern part of the study area (Figure 14; Table 3). Relative isochron thicks (120 to 150 ms TWTT) are largely contained along a pathway passing through MB1, MB2i, MB3 and MB4 (Figure 5e). The unit gradually thins southward as the unit down-laps onto the underlying SU4. There is no indication of major thinning of SU5 across the salt walls, except perhaps for subtle thinning over Salt Wall E (Figure 5e).

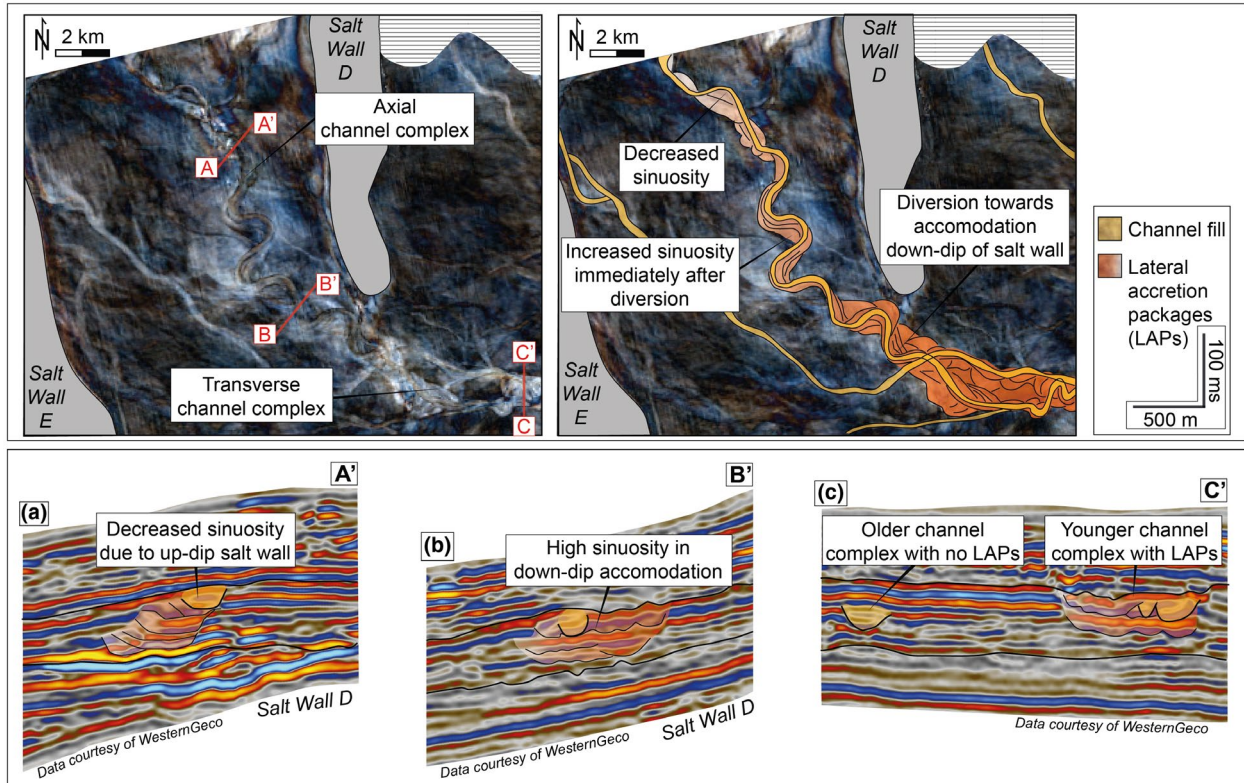
### 6.5.2 | Depositional elements

The boundary between SU4 and SU5 is marked by a notable change in seismic facies. Whereas SU4 is dominated by solitary channel complexes, SU5 is composed of thickly stacked levee-bound or erosional channel complexes, and extensive lobes. Overall SU5 comprises of 44% channel systems, 42% unconfined lobes, and 14% background deposits. Channel complexes can be further sub-divided into 40% multi-story channel complexes, 40% large erosional complexes with terraces and 20% smaller complexes with or without observable LAPs. There is one main transverse-to-structure sediment fairway for SU5, Pathway E, composed of large, stacked channel complexes and extensive lobe complexes.

### 6.5.3 | Pathway E

Pathway E comprises of three dominant channel-levee complexes with LAPs and one terminal lobe complex, these distinct sediment transport pathways ( $E_i$ ,  $E_{ii}$ ,  $E_{iii}$  and  $E_{iv}$ ) are based on relative age (oldest to youngest) and routing (Figure 14). A series of major avulsion nodes situated along the outer bends of the channel-levee systems are located along the structural highs above Salt Walls B, C, D and E (Figure 14). Avulsed channels preferentially divert northwards to form axial systems trending parallel to bounding salt structures. Two of the multi-story channel complexes ( $E_i$  and  $E_{iii}$ ) are composed of high-amplitude channel complexes up to 100 ms TWTT thick, with meander belt widths averaging 1.5 km and low- to medium-amplitude bounding levees being >2 km wide (Figures 14 and 15). The third channel complex ( $E_{iv}$ ) is erosional, c. 120 ms TWTT thick and c. 1.3 km wide, and is flanked by low-amplitude flat-topped terraces.

The oldest channel complex of Pathway E ( $E_i$ , Figure 14) is the continuation of a large stacked channel complex identified in SU4 ( $A_N$ ; Figure 11). This channel complex contains LAPs



**FIGURE 13** Uninterpreted and interpreted attribute maps showing changing channel morphology (e.g. sinuosity, meander belt width) as a channel complex is gradually diverted into accommodation down-dip of Salt Wall D within SU4 (see Figure 11 for position on map). The channel complex evolves from (c) initially a low gradient and high sinuosity system to (b) a high sinuosity system with wide meander belts in the accommodation down-dip of the salt wall, and finally to (a) a lower sinuosity system closer to a higher relief portion of the salt wall before exiting the study area

and has an average meander belt width of c. 1.2 km within MB3 (Figure 15a). This system crosses Salt Wall D and diverts northwards into an axial system within MB4, with meander belt width and sinuosity gradually decreasing (average 2.0 to 1.4 km and 1.5 to 1.3, respectively) along the minibasin (Figure 14).

Channelised lobes are the dominant component of Pathway E within MB5 and the southern portion of MB4 ( $E_{ii}$ ; Figure 14), with Pathway  $E_i$  acting as the main feeder channel. A major CLTZ for Pathway  $E_{ii}$  occurs immediately down-dip of Salt Wall D, with a series of terminal lobes developed further down-dip in MB5 (Figures 14 and 15b). Lobe geometry generally reflects the shape of the minibasin, with lobes typically being 5.4 km long and 1.8 km wide in MB5, and 7.6 km long and 1.6 km wide in the southern section of MB4. Lobe stacking patterns vary spatially throughout the minibasins, backstepping in the southern reaches of MB4, prograding over the southern tip of Salt Wall E, and mostly compensationally stacked within MB5 (Figure 14). The feathery-textured distributary channels within the lobes are diverted to trend parallel to Salt Wall  $F_i$  (Figure 14). Lobes along this pathway are also deposited to the south of the main channel complex within MB3 and MB4 with average length and width, 6.6 km and 2.9 km, respectively in these two depocentres (Figures 14 and 15a).

The penultimate major channel complex of Pathway E stems from an avulsion node above Salt Wall C ( $E_{iii}$ ; Figure 14). The meander belt width reduces after crossing Salt Wall C (from 3.1 to 1.5 km) until the channel complex reaches Salt Wall D. Here, it largely follows the structure for 17 km before diverting westwards and exiting the study area.

The youngest channel complex of Pathway E largely infills MB2i ( $E_{iv}$ ; Figure 14) and has a remarkably different geomorphology from the older major channel complexes in SU5 ( $E_i - E_{iii}$ ), with  $E_{iv}$  channels having high sinuosities (average 2.49) and having relatively wide meander belts (average 3.0 km; Figures 14 and 15c). Individual erosional channel belts are typically 250 m wide, 40 ms TWTT deep, and form elements of an extensive down-cutting channel complex that is >100 ms TWTT thick (Figure 15c).

## 7 | DISCUSSION

### 7.1 | Summary of results

The five seismic units essentially record a diminishing impact of structural topography with time within a c. 450 ms TWTT thick Late Miocene interval (Figure 16). Early



**TABLE 3** Summary of the main pathways, depositional elements and depocentres for the five seismic units

	Seismic unit	Main pathways and starting trend	Depositional elements	Depocentres
Oldest	1	A (west-trending), B (west-trending)	Solitary channel complexes (30%) and poorly imaged lobes (34%) within a dominance of background deposits (36%)	Entry points in MB2ii, southern portion of MB1 and northern portions of MB2i and MB3 (c. 60 ms TWTT)
	2	C (northwest-trending)	Dominance of extensive channel complexes (47%), with background deposits (38%) and lobes (15%)	Along main sediment pathway (up to 200 ms TWTT), notably in MB2ii. Also MB4 and MB6 (c. 130 ms TWTT)
	3	A (west-trending), B (west-trending), D (southwest-trending)	Lobes (39%), background deposits (31%), channel complexes (25%) and locally sourced MTCs (5%)	MB2i (c. 180 ms TWTT) and along sediment Pathways A and B (up to 85 ms TWTT)
	4	A (west-trending), B (west-trending), E (west-trending)	Predominately channel complexes (50%) and lobes (41%), minor background deposits (9%)	Following main central sediment pathways (up to 150 ms TWTT). Also along sediment pathways into MB5 and MB7 (c. 70 ms TWTT)
Youngest	5	E (west-trending)	Dominance of large stacked channel complexes (44%) and terminal lobes (42%), minor background deposits (14%)	Along Pathway E through MB1, MB2i, MB3 and MB4 (120 to 150 ms TWTT)

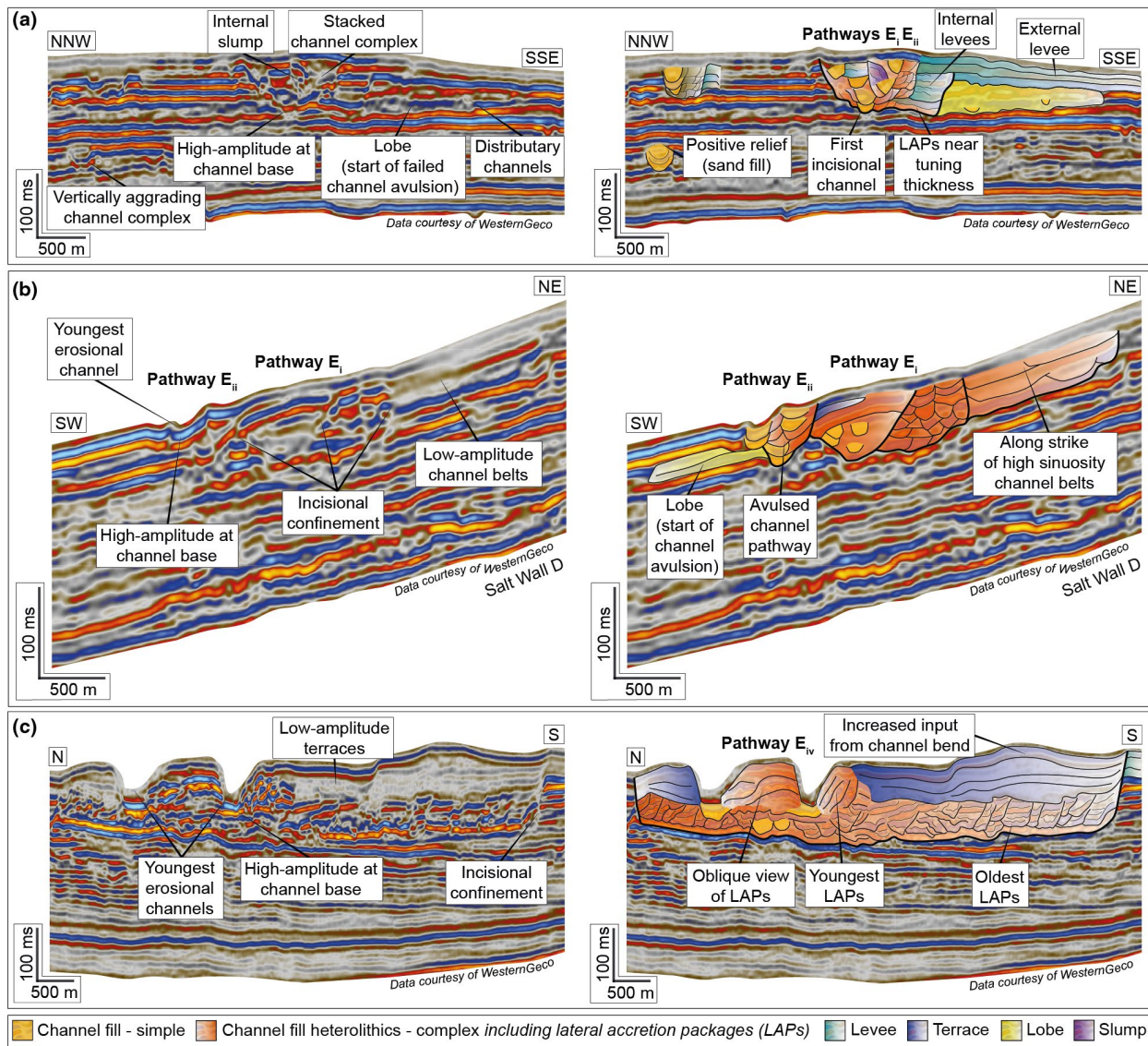
transverse-to-structure channel-lobe systems within SU1 are diverted axially northwards, but are mostly constrained to up-dip minibasins by high-relief salt walls. Extensive ponding may be encouraged by local gradient changes from high-relief down-dip salt walls, which then block the deep-water systems from exiting the minibasins (e.g. Anderson, Sickafoose, Fahrer, & Gottschalk, 2012). In contrast where sediment input is oblique-to structural strike, for example in the south-east of SU2, depositional systems are more extensive across all of the minibasins with less obvious structural influence (Figure 16a). The drastic change in sediment input locations between SU1 and SU2 is likely due to up-dip (i.e. outside of the study area) salt movement causing changes in sea-floor topography and leading to blocking and diverting the sediment routing systems. Sediment input changes again between SU2 and SU3, with the younger unit containing obliquely fed systems from the northeast and minor transversely fed systems from the east (Figure 16b). Unit depocentres subtly shift from the south of the study area towards the north and there is a substantial seismic facies evolution from relatively narrow channel complexes to a dominance of massive lobe complexes (Figure 5b,c). This is likely due to a combined salt movement re-directing major sediment routing systems outside the study area, with such high sediment accumulation along the new pathway ultimately overwhelming the salt-driven structural relief. Transverse sediment input becomes more prominent during SU4 and the sediment transport pathways are, once again, more extensive across all minibasins due to the regional slope gradient (Figure 16c). The salt wall-related structural relief is low-to-negligible at this time compared to that characterising

SU1, during which time the high-relief salt walls blocked the transverse sediment transport pathways.

Although the sediment input direction remains transverse-to-structure between SU4 and SU5, there is a major change in channel geomorphology from relatively narrow and thin low sinuosity channel complexes to wider, thicker and higher sinuosity stacked, multi-story channel complexes. The main pathway in SU5 contains three major avulsion nodes from where systems are directed northwards as channels complexes or westwards as lobe complexes (Figure 16d). The youngest channel complex in SU5 uniquely contains highly erosive and sinuous channels with adjacent low-amplitude, likely mud-rich terraces. The terraces are likely to have either formed through entrenchment or point bar accretion processes (Hansen et al., 2017). While entrenchment can occur through vertical incision or punctuated channel migration (Maier et al., 2012), point bar accretion reflects the progressive widening of channel bends within the LAPs. These channels and associated terraces are comparable to those observed by Deptuck et al. (2007), who described their development by the plug-and-cut mechanism, with erosion on the outer-bend leading to increased channel sinuosity.

The regional dip for the study area is generally towards the west (Figure 3), but there is a pattern of northward diversion of deep-water systems through the seismic units. SU1 and SU2 both display significant diversion of initially transverse channel complexes into northward-trending axial systems adjacent to the salt walls (Figure 16a,b). The youngest unit SU5 is restricted within the northern section of the study area and the major stacked channel complexes show a pattern of northward directed avulsion (Figure 16d). From a stratigraphic



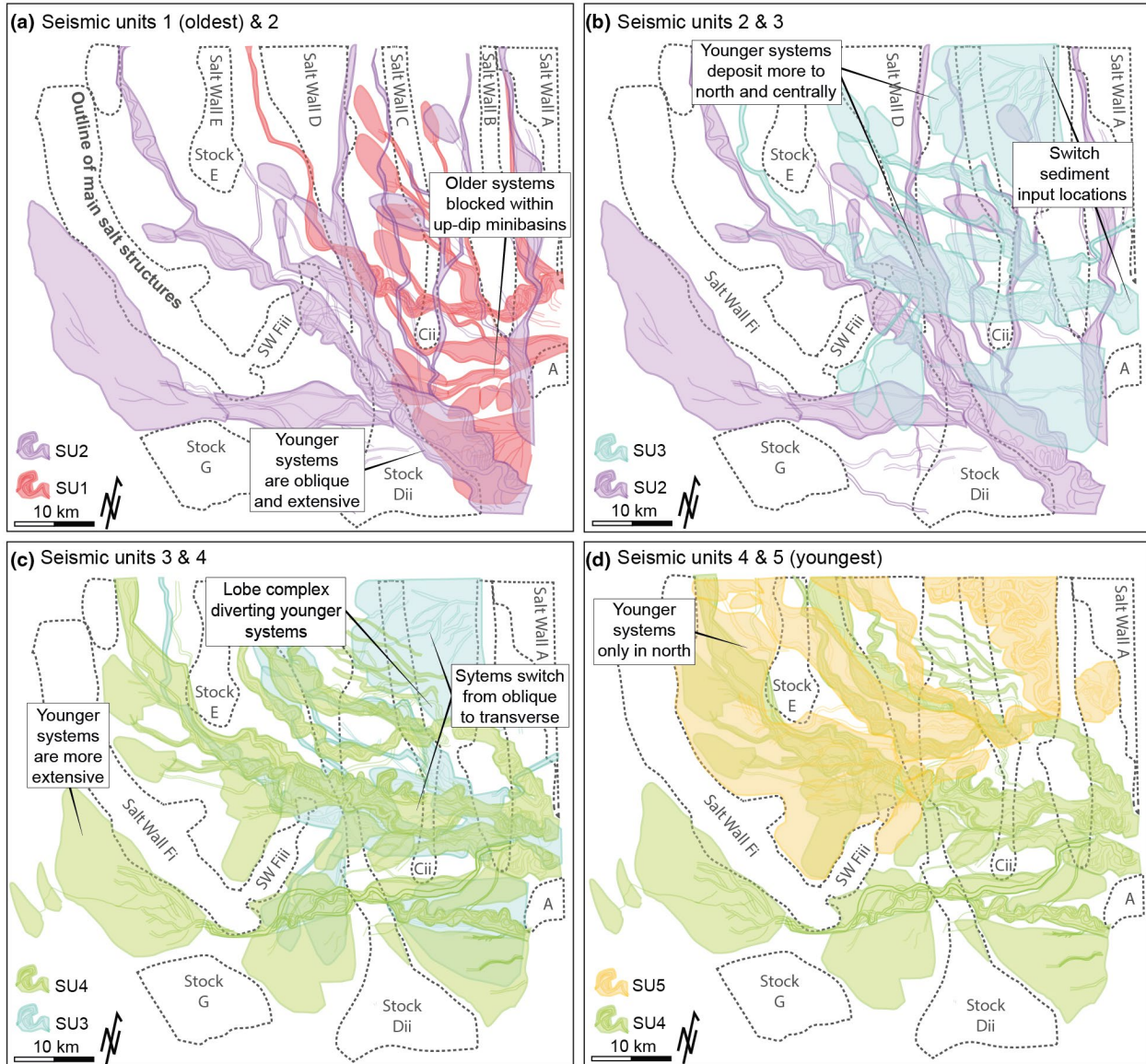


**FIGURE 15** Uninterpreted and interpreted seismic cross-sections showing the two main channel complex types and an avulsed channel pathway within SU5 (see Figure 14 for position on map). (a) Architecture of a stacked channel system along Pathway E with internal slumps, LAPs and internal/external levees. (b) Section immediately down-dip of the major avulsion node for Pathway Ei to Pathway Eii. (c) Section through Pathway Eiv showing the deeply erosive meandering channel system surrounded by low amplitude flat-topped terraces

perspective, the SU5 channel complexes can be interpreted as a compensational infill with respect to intra-basin topography related to the location of underlying SU4 systems (Figure 16d). From a structural point-of-view, it is also possible that subtle northward tilting of the slope reflects a combination of Neogene re-activation of basement fault blocks and corresponding salt movement (Hudec & Jackson, 2002, 2004). The structural gradient may also be created through the inflation of the salt plateau in the southwest of the study area. The down-dip inflated salt plateau acts as a buttress, likely creating an up-dip ‘compressional wave’ and salt squeezing of Salt Wall F and Stock F, subsequently shifting deep/water systems towards the northwest (Figures 7 and 9; Dooley, Hudec, Pichel, & Jackson, 2020).

## 7.2 | Structural growth versus sediment accumulation rate

The sediment record in tectonically active basins can be viewed in terms of the interaction between structural growth rate and sediment accumulation rate (e.g. Anderson et al., 2012; Broucke et al., 2004; Jolly et al., 2016, 2017). For example, in rift basins, different combinations of structural growth rate (rift initiation vs. rift climax) and sedimentation accumulation rate (overflow vs. starved) result in different syn-rift stratigraphic patterns (Gawthorpe & Leeder, 2000; Ravnås & Steel, 1998; Gawthorpe et al., 1994). During rift initiation, early formed fault segments and growth folds form low-relief topography, with major



**FIGURE 16** Pathway evolution between (a) the oldest pathways within SU1 and SU2, (b) SU2 and SU3, (c) SU3 and SU4, and (d) the youngest pathways within SU4 and SU5

sediment transport pathways dominated by antecedent networks leading to overfilled, to isolated depocentres. Conversely, during rift climax times, high-displacement linked faults define major, sediment-starved half grabens that are locally fed in a transverse sense by sediment derived from degrading footwall scarps, and continue as longer length-scale, through-going axial systems (Gawthorpe & Leeder, 2000). However, the complex nature of deep-water systems interacting with dynamically evolving salt tectonics makes such synthesis more difficult to achieve. Based on examples from this study and literature, we propose that the routing and geomorphology of deep-water systems can be viewed in terms of a ratio between the rate of salt structure growth or uplift and the rate of sediment accumulation (Figure 17). We define the rate of structural growth in both the regional (i.e. large-scale tectonics and regional

salt inflation) and local sense (i.e. relative sea-floor relief associated with the growth of individual salt diapirs). The ratios are for syn-kinematic deep-water systems and does not apply to pre-existing, high-relief structures that may continue to obstruct systems even during times of high sediment accumulation rate (observed influences may be similar to the left side of Figure 17). Similar relationships between the relative rates of sediment delivery and subsidence have been explored in terrestrial minibasins (Banham & Mountney, 2013).

Periods of dominantly high relative rates of structural growth relative to sediment accumulation (left side of Figure 17) have been widely documented to result in blocking, ponding or large-scale diversion on turbidite systems (e.g. Clark & Cartwright, 2009, 2012; Gee & Gawthorpe, 2006). Large-scale diversion of channel

complexes over distances  $>5$  km parallel to structural relief (e.g. SU1 Pathway A; Figure 17a) is often accompanied by a decrease in average meander belt width and sinuosity. Sometimes this major diversion can be towards segment boundaries, topographic lows between culminations of adjacent salt-cored highs (Figure 17b). Similar relationships been documented in the salt-walled minibasins of the Lower Congo Basin (Oluboyo et al., 2014). The large-relief salt-cored highs can also create substantial accommodation down-dip due to associated salt withdrawal and subsidence, which may lead to gradual channel diversion towards this topographic low and an increase in average meander belt width (Figures 13 and 17d).

Segment boundaries,  $<2$  km topographic lows, lead to a narrowing and often increase in incisional confinement of channel complexes. Down-flow of the segment boundaries channels often widen and increase in sinuosity in the down-dip minibasin (e.g. SU4 Pathway A<sub>S</sub>; Figure 17c). Chokeypoints,  $>2$  km topographic lows, can also be a major control on the location of CLTZs (e.g. SU4 Pathway A<sub>S</sub>; Figures 11 and 17e). If the unconfined flows encounter a blocking high-relief salt-cored structure down-dip, lobe complexes will deposit in the up-dip areas and likely completely infill the minibasin (e.g. SU4 Lobe A<sub>iv</sub>; Figure 17f). When the angle of incidence between the unconfined flow and strike of the structure is oblique, the lobe complex and internal distributary channels will be elongated and diverted axially, parallel to the structural strike (e.g. SU5 Pathway E<sub>ii</sub> and SU1 Pathway B; Figure 17g).

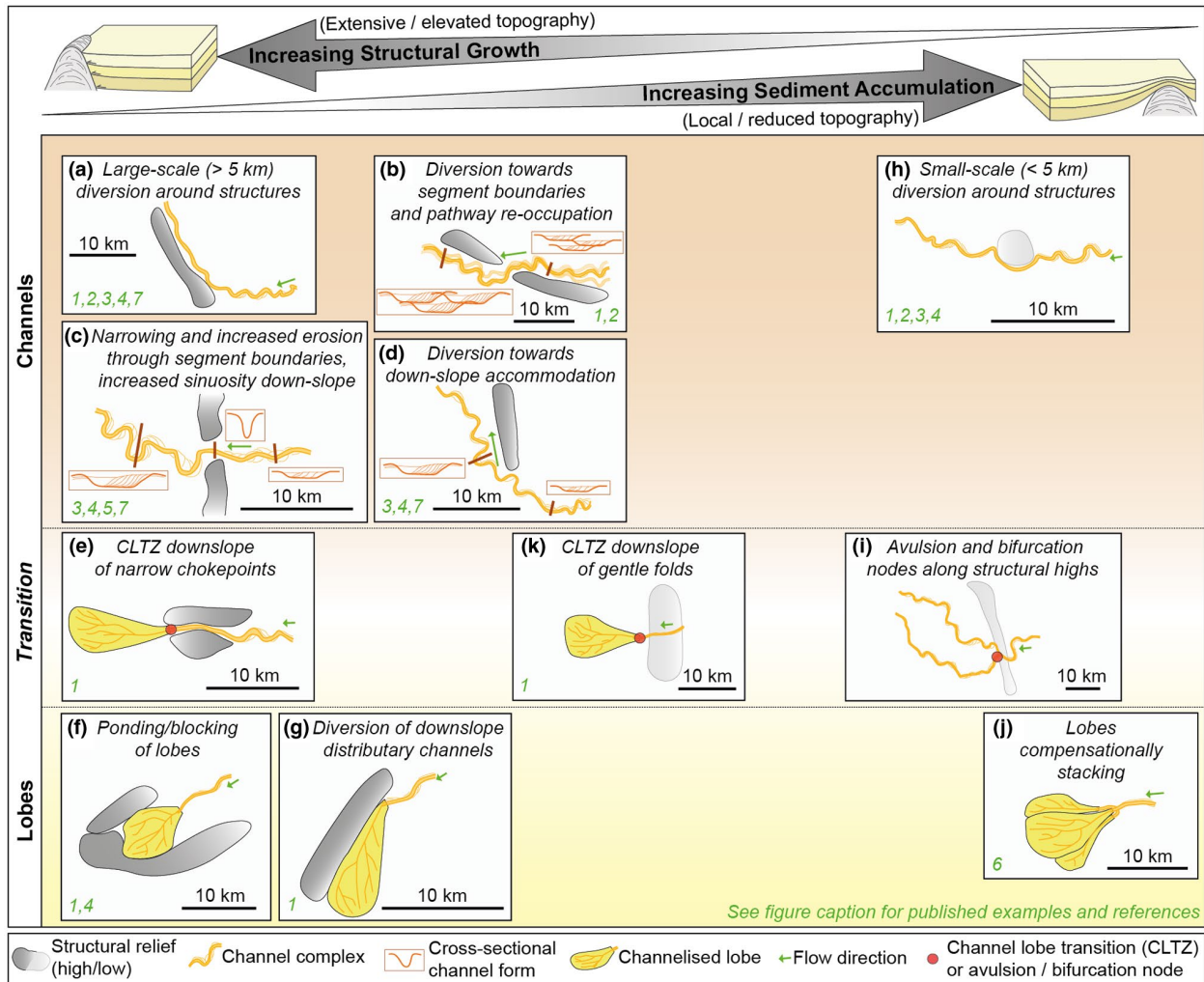
Situations characterised by where there are high rates of sediment accumulation relative to structural growth (right side of Figure 17) are commonly observed within intra-slope deep-water systems (e.g. Jobe et al., 2015). Channel complexes may be diverted small distances ( $<5$  km) around structural relief, and sinuosity may decrease slightly along the strike of the structure but increase again immediately down-dip of long-profile gradient changes (e.g. SU4 Pathway A near Stock C<sub>ii</sub>, SU1 Pathway A near Stocks C<sub>i</sub> and C<sub>ii</sub>; Figure 17h). Even when large, stacked channel complexes cross structures without showing substantial changes in trend or channel geomorphology (e.g. SU5 Pathway E over Salt Walls B, C and D), structures may still control the location of the major avulsion nodes (Figures 14 and 17i). Subtle gradient changes over fold crests (e.g. Kolla, 2007), may cause avulsion nodes to be located directly above or on the immediate down-dip flank of salt walls. Most of the avulsion nodes occur on the outside of the meander bends due to flow stripping and highest channel instability (Armitage et al., 2012). As flows tend more towards the outer channel bends, this eventually leads to flows cutting through channel confinement and depositing the initial unconfined lobes before a new channel-levee complex eventually forms (e.g. Figures 14 and 15a). When these unconfined flows encounter

little structural influence, lobe stacking patterns may be progradation or backstepping, or display compensational relationships, with a tendency towards compensational stacking (e.g. SU5 Pathway E<sub>ii</sub>; Figure 17j).

Even during periods when the rate of sediment accumulation and structural growth are broadly balanced, the latter can continue to subtly control the location of CLTZs. The CLTZ remains fixed immediately down-dip of salt walls due to the abrupt reduction of the local gradient, thereby marking the transition from major channel complex to large lobe complex (e.g. SU5 Pathway E<sub>ii</sub>; Figure 17k). This highlights the important control of subtle salt movement and local changes in gradient on deep-water depositional system evolution (centre of Figure 17), beyond the more obvious influences observed during high rates of structural growth (left side of Figure 17) or sediment accumulation (right side of Figure 17; e.g. Anderson et al., 2012).

### 7.3 | Stages of Structural Growth and Evolving Deep-water Systems

In this section we discuss the evolution of sea-floor topography and its effect on deep-water depositional systems during the typical lifespan of salt-cored structures in the contractional domain. We address this in terms of three stages of evolution: (a) initiation, (b) maturity and (c) decay (Figure 18). These growth stages can be applied to other tectonic settings (e.g. normal fault development), but the details within these stages are particularly unique to the contractional salt domain of a salt-detached slope where diapir squeezing and rejuvenation is a key control on differential subsidence and uplift, and associated sea-floor topographic evolution. Categorising the stages within the contractional salt domain is based on observations in the study area and additional studies (e.g. Oluboyo et al., 2014; Rodriguez et al., 2020), although similar salt basins characterised by a greater contribution of sediment loading, such as the Lower Congo Basin, may contain more allochthonous salt structures resulting in a more complex basin history (Anderson et al., 2012). The study interval importantly records the maturity through decay stages of salt-cored growth, as many outcrop and seismic studies focus purely on the maturity stage (e.g. Clark & Cartwright, 2012; Gee & Gawthorpe, 2006; Oluboyo et al., 2014; Pinter et al., 2018). Spatial variations within the stages is also dependent on local structural gradients being sufficient to disrupt the regional depositional gradient. Whereas salt walls within the eastern domain (e.g. Salt Walls A, B, C, D, E), gradually lose their topographical influence over time, the salt walls in the western domain (e.g. Salt Wall F<sub>i</sub>, F<sub>ii</sub>, Stocks E, D<sub>ii</sub>, G, salt plateau) are continually blocking or diverting deep-water systems over long distances with segment boundaries and chokeypoints focusing sediment transport pathways between minibasins.



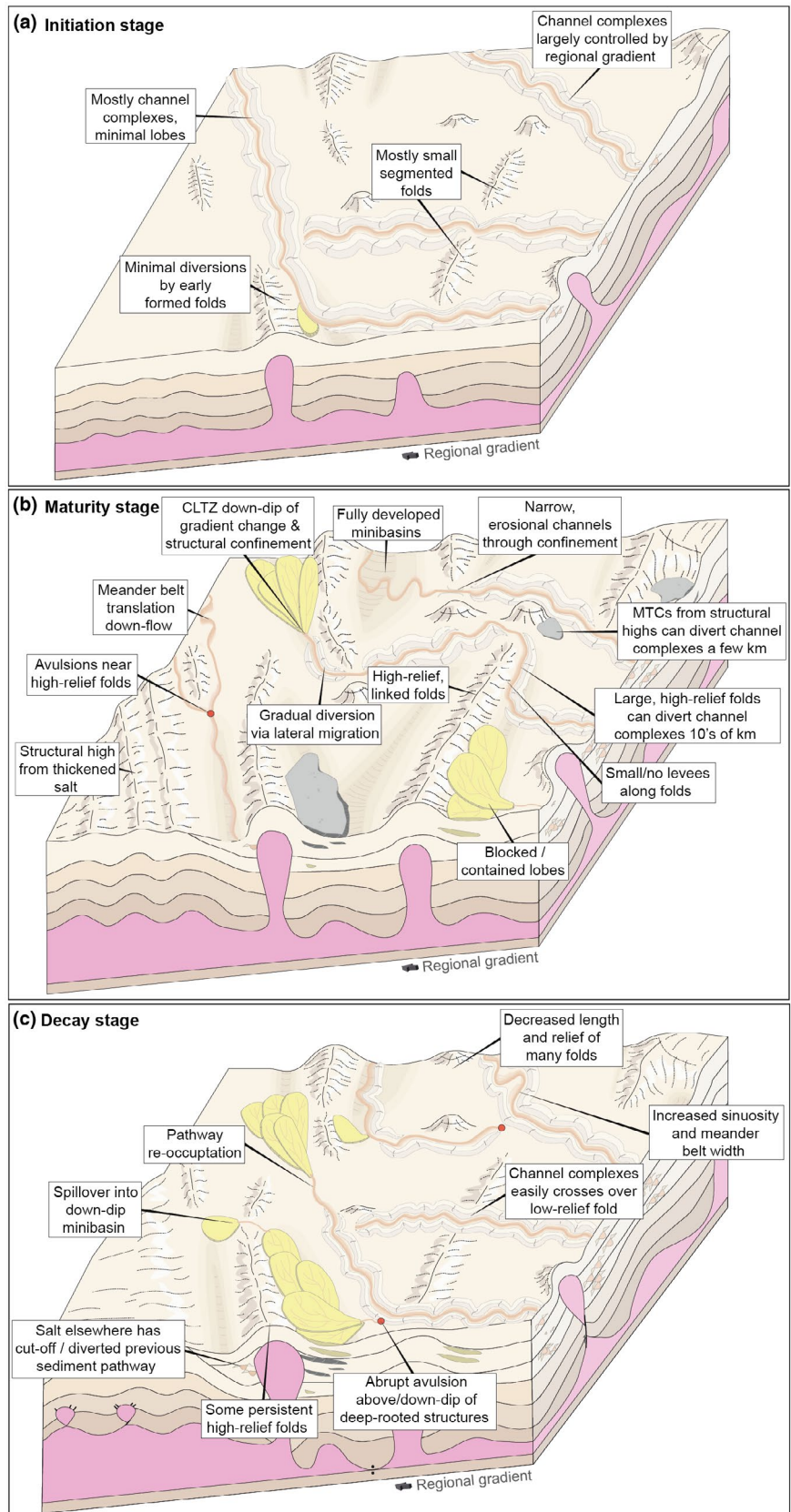
**FIGURE 17** Summary graph of the major observed influences of salt-cored structures on deep-water depositional systems. The x-axis varies from a high rate of structural growth relative to sediment accumulation on the left side (similar to the extensive and elevated salt-cored topography observed in SU1), to a low rate of structural growth relative to sedimentation accumulation on the right side (similar to the local and reduced salt-cored topography observed in SU5). The y-axis is separated into channels (top) transitioning into channel-lobe transition zones or avulsion nodes (middle) through to lobes (bottom). Each sketch box contains selected reference examples: 1 (Oluboyo et al., 2014), 2 (Mayall et al., 2010), 3 (Gee & Gawthorpe, 2006), 4 (Clark & Cartwright, 2009; Clark & Cartwright, 2011), 5 (Hay, 2012), 6 (Doughty-Jones et al., 2017), 7 (Anderson et al., 2012)

The initiation, or early syn-kinematic, stage is characterised by the early growth of low-relief, segmented salt-cored structures that create minor diversions of channel-lobe systems as the systems are mainly influenced by the regional margin gradient (Figure 18a). The record of geomorphological and sediment routing changes due to minor structurally controlled sea-floor rugosity may be difficult to recognise as the turbidite systems extend across and between several minibasins. The limited diversion of turbidite systems are due to early formed fold-related topography. There are few lobe complexes due to a lack of gradient changes and confining minibasins, thereby channel complexes are the most abundant deep-water element during this stage (Figure 18a). The channels move gradually in response to structural growth through lateral migration, but overall establishment of these

early developed sediment transport pathways during the initiation stage are important for the maturity and decay stages, given they often persist for a longtime (e.g. Pathways A and B). This is observed in other salt basins when the erosional capabilities of the channel complexes are greater than the rate of structural growth (Mayall et al., 2010).

The maturity, or main syn-kinematic, stage is distinguished by high-relief, laterally linked salt-cored highs that are capable of blocking and diverting channel-lobe systems in some minibasins. Some minibasins may be sediment starved if they lie in 'shadow zones' with respect to the main sediment transport pathways (Figure 18b; Oluboyo et al., 2014). Large elongate salt walls separate fully developed minibasins that confine flows and contain mostly axial channel-lobe systems. Segment boundaries and chokepoints

**FIGURE 18** Dynamic evolution of submarine channel-lobe systems and salt-cored structures within the contractional salt domain from the (a) initiation or development stage, largely controlled by the regional margin gradient and consisting of low-relief, segmented salt-cored structures, to the (b) maturity stage, comprised of linked, high relief salt-cored structures and well-defined minibasins, and finally to the (c) decay stage where many structures have substantially diminished in length and relief relative to sedimentation rate. See text for more detailed descriptions



developed between major salt-cored structures result in long-lived sediment transport pathways if sediment accumulation in the up-dip is sufficient to overcome the spill point through

the segment boundary; this may also potentially control the location of the major CLTZ (Figure 18b). An indirect influence of the high structural relief created during the maturity

stage is topographic complexity around localised MTCs derived from degradation of fold flanks (e.g. Figures 10b,c and 18b; Wu et al., 2020). Whereas extensive MTCs on active plate margins have been shown to cause substantial diversions of channel complexes and control avulsion nodes (e.g. Olafiranye et al., 2013; Ortiz-Karpf et al., 2017; Zhao et al., 2019), the MTCs within this study interval are present as relatively small (18 km<sup>2</sup>) and thin (c. 40 ms TWTT) deposits sourced from local salt-cored highs. Although the MTCs may cause minor diversion of channel complexes, they have a more material impact on decreasing meander belt width and sinuosity. Differential compaction of older deposits, such as lobe complexes (e.g. Pathway D in Figure 9; Pathway E in Figure 10a) and channel complexes (e.g. Pathway A<sub>ii</sub> in Figure 10b,c) also influences sea-floor topography within minibasins, thereby influencing the routing of channel-lobe systems.

The final decay, or late syn-kinematic, stage contains linked long-lived structures with diminished sea-floor relief due to sediment accumulation outpacing structural growth rate (Figure 18c). The decay or 'death' stage has been documented for normal faults (Jackson, 1999), but is comparably understudied for salt domains. Minibasins subside less strongly during this time due to reduced salt migration and eventual welding. Salt walls associated with subtle-to-negligible syn-depositional sea-floor allows channel complexes to cross highs that previously blocked or diverted turbidite systems. As topographic differentiation reduces routing of deep-water systems, some channel complexes may continue into and deposit within previous 'shadow zones' formed during the maturity stage. As sediment accumulation rate is greater than the growth of structures, structural controls on channel-lobe systems is more subtle. During the decay stage channel movement may be mostly abrupt via avulsions rather than gradual lateral migration (e.g. major avulsion nodes in Figure 14 vs. channel complex diversion into accommodation in Figure 13), as gradual diversion is a response of the deep-water systems to actively growing salt-cored structures. Instead, in the decay stage, subtle structural highs control major avulsion nodes along or immediately down-dip of fold flanks due to occasional re-activation of salt movement through squeezing (Figure 18c). Differential compaction of thicker minibasin fill (>200 m burial sensu Ward et al., 2017) may also play an important role in controlling avulsion node localities through creating gradual gradients. Although most of the salt-cored structures are low-relief during this stage, some large structures may be long-lived and continue blocking sediment transport pathways and ponding sediments (Figure 18c). These long-lived structures may have developed enough topography in the early stages and are able to retain their positive topographic expression relative

to adjacent minibasins (e.g. down-dip salt plateau and Salt Wall F). Alternatively, these long-lived structures may continue to grow, or experience intermittent salt movement, as other structures decay (e.g. Anderson et al., 2012; Mayall et al., 2010).

## 8 | CONCLUSIONS

Evolving salt tectonics and corresponding sea-floor topography along salt-influenced passive margins impacts the routing and geomorphology of submarine channel-lobe systems on a regional-scale. Detailed mapping of the evolution of Late Miocene systems from the Kwanza Basin, offshore Angola has helped us to understand the location and character of channel-lobe systems and major avulsion nodes, in relation to developing structurally controlled sea-floor topography during initiation, maturity and decay stages of salt-cored folds and minibasin depocentres. The geomorphology, stacking and internal architecture of deep-water channel-lobe systems can be understood in terms of the ratio between structural growth rate and sediment accumulation rate.

Initially, high-relief salt-cored structures confine channel-lobe systems to the up-dip minibasins through large-scale diversion of transverse-to-structure channel complexes, with segment boundaries localising sediment transport pathways between adjacent minibasins. Major salt-cored structures control the location of channel-lobe transition zones to immediately down-dip of segment boundaries, chokepoints and structural gradient changes across salt wall crests. The youngest units only display subtle structural topography and the expression of the salt-cored structures diminishes with time. Low-relief structures still influence turbidite systems through small-scale diversion and by controlling the location of avulsion above remnant structural highs. Control on avulsion nodes is likely due to brief periods of minor rejuvenated salt movement during times of dominating sediment accumulation and/or subtle inherited gradients from differential compaction. Channels in these structurally active settings are re-routed both abruptly, in response to structural growth via avulsion nodes, and gradually, through lateral migration.

The results of this study combined with observations in other salt-influenced margins have allowed us to develop generic models of the tectono-sedimentary response of deep-water depositional systems in contractional salt domains in terms of three general stages of structural growth: initiation, maturity and decay. The initiation stage is characterised by low-relief, segmented salt-cored structures and poorly defined minibasins, allowing channel complexes to largely follow the regional margin gradient with minimal diversions

or ponding of unconfined flows. The maturity stage is characterised by elongate, high-relief salt-cored highs expressed as folds on the sea-floor, leading to large-scale axial diversion of channel complexes along structural strike and funnelling of depositional systems through segment boundaries and chokepoints. Ponded channel-lobe systems and MTCs derived from local fold flanks are also commonly deposited in the well-developed minibasins. During the decay stage, structural relief gradually diminishes as sediment accumulation begins to outpace structural growth. This leads to a more complex array of through-going channel-lobe systems with occasional blocking.

The results of this paper contribute to the understanding of the structural controls and the variability of to channel-lobe systems during the stages of structural growth that can be applied to similar settings containing salt-influenced minibasins. The results of the study also highlight complications due to strong local structural gradients and the varying angle of incidence between the deep-water system and structural strike, which drastically impacts on the degree of blocking and diversion, as well as the tendency of sediment routing systems to be orientated transverse or axial to structure.

#### ACKNOWLEDGEMENTS

This study is part of the first author's PhD project, which is supported by the Turbidites, Topography and Tectonics (T3) project funded by Equinor. We especially thank Michal Warchol, Michal Janocko and Frode Hadler-Jacobsen for their thoughtful feedback and discussion over the years. We acknowledge WesternGeco for providing access to the seismic reflection survey and giving permission to publish in this paper. Constructive reviews by Mike Mayall, Ian Clark, an anonymous reviewer and Associate Editor Cari Johnson are gratefully acknowledged. We also thank Schlumberger, Eliis and Geoteric for providing software under educational licenses to the 3D seismic lab at the University of Bergen. Gawthorpe acknowledges VISTA for funding the VISTA Professorship.

#### CONFLICT OF INTEREST

The authors have no conflict of interest to declare.

#### PEER REVIEW

The peer review history for this article is available at <https://publons.com/publon/10.1111/bre.12506>.

#### DATA AVAILABILITY STATEMENT

The data that support the findings of this study are available from WesternGeco. Restrictions apply to the availability of these data, which were used under license for this study. Data are available from the authors with the permission of WesternGeco.


#### ORCID

Danielle M. Howlett  <https://orcid.org/0000-0001-6680-2282>

Rob L. Gawthorpe  <https://orcid.org/0000-0002-4352-6366>

Zhiyuan Ge  <https://orcid.org/0000-0002-6029-5512>

Atle Rotevatn  <https://orcid.org/0000-0002-8413-3294>

Christopher A.-L. Jackson  <https://orcid.org/0000-0002-8592-9032>

#### REFERENCES

- Aas, T. E., Basani, R., Howell, J. A., & Hansen, E. (2014). Forward modelling as a method for predicting the distribution of deep-marine sands: an example from the Peira Cava Sub-Basin. In A. W. Martinius, J. A. Howell and T. R. Good, (Eds.), *Sediment-Body Geometry and Heterogeneity: Analogue Studies for Modelling the Subsurface*. Geological Society, London, *Special Publications*, 387, 247–269.
- Abreu, V., Sullivan, M., Pirmez, C., & Mohrig, D. (2003). Lateral accretion packages (Laps): An important reservoir element in deep water sinuous channels. *Marine and Petroleum Geology*, 20, 631–648.
- Anderson, A. V., Sickafosse, D. K., Fahrner, T. R., & Gottschalk, R. R. (2012). Interaction of Oligocene–Miocene deep-water depositional systems with actively evolving structures: The Lower Congo Basin, offshore Angola. In D. Gao (Ed.), *Tectonics and sedimentation: Implications for petroleum systems*. *AAPG Memoir*, 100, 291–313.
- Anderson, J. E., Cartwright, J., Drysdall, S. J., & Vivian, N. (2000). Controls on turbidite sand deposition during gravity-driven extension of a passive margin: Examples from miocene sediments in block 4, Angola. *Marine and Petroleum Geology*, 17, 1165–1203.
- Armitage, D. A., Mchargue, T., Fildani, A., & Graham, S. A. (2012). Postavulsion Channel Evolution: Niger Delta Continental Slope. *AAPG Bulletin*, 96, 823–843.
- Banham, S. G., & Mountney, N. P. (2013). Evolution of fluvial systems in salt-walled mini-basins: A review and new insights. *Sedimentary Geology*, 296, 142–166.
- Basani, R., Janocko, M., Cartigny, M. J. B., Hansen, E. W. M., & Eggenhuisen, J. T. (2014). Massflow-3d as a simulation tool for turbidity currents: some preliminary results. In: A. W. Martinius, R. Ravnas, J. A. Howell, R. J. Steel & J. P. Wonham (Eds.), *From Depositional Systems to Sedimentary Successions on the Norwegian Continental Margin*. *IAS Special Publication*, 46, 587–608.
- Boulestex, K., Poyatos-Moré, M., Flint, S. S., Taylor, K. G., Hodgson, D. M., & Hasiotis, S. T. (2019). Transport and deposition of mud in deep-water environments: processes and stratigraphic implications. *Sedimentology*, 66, 2894–2925.
- Brice, S. E., Cochran, M. D., Pardo, G., & Edwards, A. D. (1982). *Tectonics and sedimentation of the south atlantic rift sequence*. Cabinda, Angola Rifted Margins: Field Investigations of Margin Structure and Stratigraphy.
- Brooks, H., Hodgson, D., Brunt, R. L., Peakall, J., Hofstra, M. & Flint, S., (2018). Deep-water channel-lobe transition zone dynamics: Processes and depositional architecture, an example from the Karoo Basin, South Africa. *GSA Bulletin*, 130, 1723–1746.
- Broucke, O., Temple, F., Rouby, D., Robin, C., Calassou, S., Nalpas, T., & Guillocheau, F. (2004). The role of deformation processes on the geometry of mud-dominated turbiditic systems, Oligocene

- and lower-middle Miocene of the lower Congo Basin (West African Margin). *Marine and Petroleum Geology*, *21*, 327–348.
- Brown, A. R. (1991). Interpretation of three-dimensional seismic data. *AAPG Memoir*, *42*, 341.
- Brownfield, M. E., & Charpentier, R. R. (2006). Geology and total petroleum systems of the west-central coastal province (7203), West Africa U.S. Geological Survey Bulletin. 2207-B, 52 p.
- Brun, J.-P., & Fort, X. (2011). Salt tectonics at passive margins: geology versus models. *Marine and Petroleum Geology*, *28*, 1123–1145.
- Bull, S., Cartwright, J., & Huuse, M. (2009). A review of kinematic indicators from mass-transport complexes using 3D seismic data. *Marine and Petroleum Geology*, *26*, 1132–1151.
- Cartigny, M. J. B., Eggenhuisen, J. T., Hansen, E. W. M., & Postma, G. (2013). Concentration-dependent flow stratification in experimental high-density turbidity currents and their relevance to turbidite facies models. *Journal of Sedimentary Research*, *83*, 1046–1064.
- Clark, I. R., & Cartwright, J. A. (2009). Interactions between Submarine channel systems and deformation in deepwater fold belts: Examples from the Levant Basin, Eastern Mediterranean Sea. *Marine and Petroleum Geology*, *26*, 1465–1482.
- Clark, I. R., & Cartwright, J. A. (2011). Key controls on submarine channel development in structurally active settings. *Marine and Petroleum Geology*, *28*, 1333–1349. <http://dx.doi.org/10.1016/j.marpetgeo.2011.02.001>
- Clark, I. R., & Cartwright, J. A. (2012). Interactions between Coeval Sedimentation and Deformation from the Niger Delta Deepwater Fold Belt. In: B. E. Prather, M. E. Deptuck, D. Mohrig, B. van Hoorn & R. B. Wynn (Eds.), Application of the Principles Seismic Geomorphology to Continental Slope and Base-of-slope Systems: Case Studies from Seafloor and Near-Seafloor Analogues. *SEPM Special Publication*, 243–267.
- Collinson, J. D., & Thompson, D. B. (1982). *Sedimentary Structures* (p. 194). London: George Allen & Unwin.
- Deptuck, M. E., Steffens, G. S., Barton, M., & Pirmez, C. (2003). Architecture and evolution of upper fan channel-belts on the niger delta slope and in the Arabian Sea. *Marine and Petroleum Geology*, *20*, 649–676.
- Deptuck, M. E., Sylvester, Z., Pirmez, C., & O'byrne, C. (2007). Migration-aggradation history and 3D seismic geomorphology of submarine channels in the pleistocene benin-major canyon, western niger delta slope. *Marine and Petroleum Geology*, *24*, 406–433.
- Dooley, T. P., Hudec, M. R., Pichel, L. M., & Jackson, M. P. A. (2020). The impact of base-salt relief on salt flow and suprasalt deformation patterns at the autochthonous, paraautochthonous and allochthonous level: Insights from physical models. *Geological Society, London, Special Publications*, *476*, 287–315.
- Doughty-Jones, G., Lonergan, L., Mayall, M., & Dee, S. (2019). The role of structural growth in controlling the facies and distribution of mass transport deposits in a deep-water salt minibasin. *Marine and Petroleum Geology*, *104*, 106–124.
- Doughty-Jones, G., Mayall, M., & Lonergan, L. (2017). Stratigraphy, facies, and evolution of deep-water lobe complexes within a salt-controlled intraslope minibasin. *AAPG Bulletin*, *101*, 1879–1904. <https://doi.org/10.1306/01111716046>
- Duval, B., Cramez, C., & Jackson, M. P. A. (1992). Raft tectonics in the Kwanza Basin, Angola. *Marine and Petroleum Geology*, *9*, 389–404. [https://doi.org/10.1016/0264-8172\(92\)90050-O](https://doi.org/10.1016/0264-8172(92)90050-O)
- Eggenhuisen, J. T., & McCaffrey, W. D. (2012). The vertical turbulence structure of experimental turbidity currents encountering basal obstructions: implications for vertical suspended sediment distribution in non-equilibrium currents. *Sedimentology*, *59*, 1101–1120. <https://doi.org/10.1111/j.1365-3091.2011.01297.x>
- Fort, X., Brun, J. P., & Chauvel, F. (2004). Salt tectonics on the angolan margin, synsedimentary deformation processes. *AAPG Bulletin*, *88*, 1523–1544. <https://doi.org/10.1306/06010403012>
- Gamberi, F., & Rovere, M. (2011). Architecture of a modern transient slope fan (Villafranca Fan, Gioia Basin-Southeastern Tyrrhenian Sea). *Sedimentary Geology*, *236*, 211–225. <https://doi.org/10.1016/j.sedgeo.2011.01.007>
- Gamboa, D., & Alves, T. M. (2015). Spatial and dimensional relationships of submarine slope architectural elements: A seismic-scale analysis from the Espírito Santo Basin (SE Brazil). *Marine and Petroleum Geology*, *64*, 43–57. <https://doi.org/10.1016/j.marpetgeo.2015.02.035>
- Gawthorpe, R. L., Fraser, A. J., & Collier, R. E. L. (1994). Sequence stratigraphy in active extensional basins: Implications for the interpretation of ancient basin-fills. *Marine and Petroleum Geology*, *11*, 642–658. [https://doi.org/10.1016/0264-8172\(94\)90021-3](https://doi.org/10.1016/0264-8172(94)90021-3)
- Gawthorpe, R. L., & Leeder, M. R. (2000). Tectono-sedimentary evolution of active extensional basins. *Basin Research*, *12*, 195–218. <https://doi.org/10.1046/j.1365-2117.2000.00121.x>
- Ge, Z., Nemeč, W., Gawthorpe, R. L., Rotevatn, A., & Hansen, E. W. M. (2018). Response of unconfined turbidity current to relay-ramp topography: insights from process-based numerical modelling. *Basin Research*, *30*, 321–343. <https://doi.org/10.1111/bre.12255>
- Gee, M. J. R., & Gawthorpe, R. L. (2006). Submarine channels controlled by salt tectonics: Examples from 3D seismic data offshore Angola. *Marine and Petroleum Geology*, *23*, 443–458. <https://doi.org/10.1016/j.marpetgeo.2006.01.002>
- Gee, M. J. R., Gawthorpe, R. L., Bakke, K., & Friedmann, S. J. (2007). Seismic geomorphology and evolution of submarine channels from the Angolan continental margin. *Journal of Sedimentary Research*, *77*, 433–446. <https://doi.org/10.2110/jsr.2007.042>
- Giles, K. A., & Rowan, M. G. (2012). Concepts in halokinetic-sequence deformation and stratigraphy. In: G. I. Alsop, S. G. Archer, A. J. Hartley, N. T. Grant & R. Hodgkinson (Eds.), Salt Tectonics, Sedimentation and Prospectivity. *Geological Society, London, Special Publications*, *363*, 7–31.
- Guiraud, M., Buta-Neto, A., & Quesne, D. (2010). Segmentation and differential post-rift uplift at the angola margin as recorded by the transform-rifted benguela and oblique-to-orthogonal-rifted kwanza basins. *Marine and Petroleum Geology*, *27*, 1040–1068. <https://doi.org/10.1016/j.marpetgeo.2010.01.017>
- Guiraud, R., & Maurin, J. C. (1992). Early Cretaceous rifts of western and central Africa: An overview. *Tectonophysics*, *213*, 153–168. [https://doi.org/10.1016/0040-1951\(92\)90256-6](https://doi.org/10.1016/0040-1951(92)90256-6)
- Hadler-Jacobsen, F., Gardner, M. H., & Borer, J. M. (2007). Seismic stratigraphic and geomorphic analysis of deep-marine deposition along the west african continental margin. In R. J. Davies, H. W. Posamentier, L. J. Wood & J. A. Cartwright (Eds.), Seismic geomorphology: Applications to hydrocarbon exploration and production. *Geological Society, London, Special Publications*, *277*, 47–84.
- Hadler-Jacobsen, F., Johannessen, E. P., Ashton, N., Henriksen, S., Johnson, S. D., & Kristensen, J. B. (2005). Submarine fan morphology and lithology distribution: A predictable function of sediment delivery, gross shelf-to-basin relief, slope gradient and basin topography. *Geological Society, London, Petroleum Geology Conference Series*, *6*, 1121–1146. <https://doi.org/10.1144/0061121>



- Hansen, L., Janocko, M., Kane, I., & Kneller, B. (2017). Submarine channel evolution, terrace development, and preservation of intra-channel thin-bedded turbidites: Mahin and Avon channels. *Offshore Nigeria. Marine Geology*, 383, 146–167. <https://doi.org/10.1016/j.marpetgeo.2016.11.011>
- Haughton, P. D. W. (2000). Evolving turbidite systems on a deforming basin floor, Tabernas, SE Spain. *Sedimentology*, 47, 497–518. <https://doi.org/10.1046/j.1365-3091.2000.00293.x>
- Hay, D. C. (2012). Stratigraphic evolution of a tortuous corridor from the stepped slope of Angola. In E. Bradford, M. D. Prather, D. Mohrig, B. Van Hoorn & R. B. Wynn (Eds.), Application of the principles of seismic geomorphology to continental-slope and base-of-slope systems: case studies from seafloor and near-seafloor analogues. *SEPM Special Publication*, 99, 163–180.
- Hofstra, M., Hodgson, D. M., Peakall, J., & Flint, S. S. (2015). Giant scour-fills in ancient channel-lobe transition zones: formative processes and depositional architecture. *Sedimentary Geology*, 329, 98–114. <https://doi.org/10.1016/j.sedgeo.2015.09.004>
- Howlett, D. M., Ge, Z., Nemec, W., Gawthorpe, R. L., Rotevatn, A., & Jackson, C. A. L. (2019). Response of unconfined turbidity current to deep-water fold and thrust belt topography: orthogonal incidence on solitary and segmented folds. *Sedimentology*, 66, 2425–2454. <https://doi.org/10.1111/sed.12602>
- Hudec, M. R., & Jackson, M. P. A. (2002). Structural segmentation, inversion, and salt tectonics on a passive margin: Evolution of the inner Kwanza Basin, Angola. *GSA Bulletin*, 114, 1222–1244. [https://doi.org/10.1130/0016-7606\(2002\)114<1222:SSIAST>2.0.CO;2](https://doi.org/10.1130/0016-7606(2002)114<1222:SSIAST>2.0.CO;2)
- Hudec, M. R., & Jackson, M. P. A. (2004). Regional restoration across the Kwanza Basin, Angola: salt tectonics triggered by repeated uplift of a metastable passive margin. *AAPG Bulletin*, 88, 971–990. <https://doi.org/10.1306/02050403061>
- Hudec, M. R., & Jackson, M. P. A. (2007). Terra Infirma: understanding salt tectonics. *Earth Science Reviews*, 82, 1–28.
- Jackson, C. A. L., & Lewis, M. M. (2012). Origin of an anhydrite sheath encircling a salt diapir and implications for the seismic imaging of steep-sided salt structures, Egersund Basin, Northern North Sea. *Journal of the Geological Society*, 169(5), 593–599. <https://doi.org/10.1144/0016-76492011-126>
- Jackson, J. (1999). Fault Death: A perspective from actively deforming regions. *Journal of Structural Geology*, 21, 1003–1010. [https://doi.org/10.1016/S0191-8141\(99\)00013-9](https://doi.org/10.1016/S0191-8141(99)00013-9)
- Jackson, M. P. A., Hudec, M. R., & Hegarty, K. A. (2005). The great West African Tertiary coastal uplift: Fact or fiction? A perspective from the angolan divergent margin. *Tectonics*, 24, 1–23. <https://doi.org/10.1029/2005TC001836>
- Janocko, M., Nemec, W., Henriksen, S., & Warcho, M. (2013). The diversity of deep-water sinuous channel belts and slope valley-fill complexes. *Marine and Petroleum Geology*, 41, 7–34. <https://doi.org/10.1016/j.marpetgeo.2012.06.012>
- Jian-Ping, L. I. U., Pan, X. H., Jun, M., Tian, Z. J., Chen, Y. J. W., & Wan, L.-K. (2008). Petroleum geology and resources in West Africa: An overview. *Petroleum Exploration and Development*, 35, 378–383. [https://doi.org/10.1016/S1876-3804\(08\)60086-5](https://doi.org/10.1016/S1876-3804(08)60086-5)
- Jobe, Z. R., Sylvester, Z., Parker, A. O., Howes, N., Slowey, N., & Pirmez, C. (2015). Rapid adjustment of submarine channel architecture to changes in sediment supply. *Journal of Sedimentary Research*, 85, 729–753. <https://doi.org/10.2110/jsr.2015.30>
- Jolly, B., Lonergan, L., & Whittaker, A. (2016). Growth history of fault-related folds and interaction with seabed channels in the toe-thrust region of the deep-water Niger Delta. *Marine and Petroleum Geology*, 70, 58–76. <https://doi.org/10.1016/j.marpetgeo.2015.11.003>
- Jolly, B., Whittaker, A., & Lonergan, L. (2017). Quantifying the geomorphic response of modern submarine channels to actively growing folds and thrusts, deep-water Niger Delta. *GSA Bulletin*, 129, 1123–1139. <https://doi.org/10.1130/B31544.1>
- Jones, I. F., & Davison, I. (2014). Seismic Imaging in and around Salt Bodies. *Interpretation*, 2, SL1–SL20. <https://doi.org/10.1190/INT-2014-0033.1>
- Karner, G. D., & Driscoll, N. W. (1999). Tectonic and stratigraphic development of the West African and Eastern Brazilian Margins: Insights from quantitative basin modelling. In N. R. Cameron, R. H. Bate & V. S. Clure (Eds.), The oil and gas habitats of the South Atlantic. *Geological Society, London, Special Publications*, 153, 11–40.
- Kneller, B. (1995). Beyond the turbidite paradigm: physical models for deposition of turbidites and their implications for reservoir prediction. In A. J. Hartley and D. J. Prosser (Eds.), Characterization of deep marine clastic systems. *Geological Society, London, Special Publications*, 94, 31–49.
- Kneller, B., Edwards, D., Mccaffrey, W., & Moore, R. (1991). Oblique reflection of turbidity currents. *Geology*, 19, 250–252. [https://doi.org/10.1130/0091-7613\(1991\)019<0250:OROTC>2.3.CO;2](https://doi.org/10.1130/0091-7613(1991)019<0250:OROTC>2.3.CO;2)
- Kneller, B. C., & Mccaffrey, W. D. (1995). Modelling the effects of salt-induced topography on deposition from turbidity currents. *Salt, Sediment and Hydrocarbons: Gulf Coast Section SEPM*, 1, 137–145.
- Kolla, V. (2007). A review of sinuous channel avulsion patterns in some major deep-seafans and factors controlling them. *Marine and Petroleum Geology*, 24, 450–469. <https://doi.org/10.1016/j.marpetgeo.2007.01.004>
- Lavier, L. L., Steckler, M. S., & Brigaud, F. (2001). Climatic and tectonic control on the cenozoic evolution of the West African Margin. *Marine Geology*, 178, 63–80.
- Liu, Q., Kneller, B., Fallgatter, C., Valdez Buso, V., & Milana, J. P. (2018). Tabularity of individual turbidite beds controlled by flow efficiency and degree of confinement. *Sedimentology*, 65, 2368–2387. <https://doi.org/10.1111/sed.12470>
- Lundin, E. R. (1992). Thin-skinned extensional tectonics on a salt detachment, Northern Kwanza Basin, Angola. *Marine and Petroleum Geology*, 9, 405–411. [https://doi.org/10.1016/0264-8172\(92\)90051-F](https://doi.org/10.1016/0264-8172(92)90051-F)
- Maestrelli, D., Iacopini, D., Jihad, A. A., Bond, C. E., & Bonini, M. (2017). Seismic and structural characterization of fluid escape pipes using 3d and partial stack seismic from the loyal field (Scotland, UK): A multiphase and repeated intrusive mechanism. *Marine and Petroleum Geology*, 88, 489–510. <https://doi.org/10.1016/j.marpetgeo.2017.08.016>
- Maier, K. L., Fildani, A., Mchargue, T. R., Paull, C. K., Graham, S. A., & Caress, D. W. (2012). Punctuated deep-water channel migration: high-resolution subsurface data from the lucia chica channel system, offshore California, U.S.A. *Journal of Sedimentary Research*, 82, 1–8. <https://doi.org/10.2110/jsr.2012.10>
- Martinez, J. F., Cartwright, J., & Hall, B. (2005). 3d Seismic interpretation of slump complexes: Examples from the continental margin of Israel. *Basin Research*, 17, 83–108. <https://doi.org/10.1111/j.1365-2117.2005.00255.x>
- Marton, L. G. (2000). Evolution of the Angolan passive margin, West Africa, with emphasis on post-salt structural styles. In W. Mohriak & M. Talwani (Eds.), Atlantic Rifts and Continental Margins. *The American Geophysical Union Washington*, 115, 129–149.

- Mattos, N. H., Alves, T. M., & Scully, A. (2019). Structural and depositional controls on plio-pleistocene submarine channel geometry (Taranaki Basin, New Zealand). *Basin Research*, *31*, 136–154. <https://doi.org/10.1111/bre.12312>
- Mayall, M., Lonergan, L., Bowman, A., James, S., Mills, K., Primmer, T., ... Skeene, R. (2010). The response of turbidite slope channels to growth-induced seabed topography. *AAPG Bulletin*, *94*, 1011–1030. <https://doi.org/10.1306/01051009117>
- Mcardle, N. J., & Ackers, M. A. (2012). Understanding seismic thin-bed responses using frequency decomposition and RGB blending. *First Break*, *30*, 57–65. <https://doi.org/10.3997/1365-2397.2012022>
- Moulin, M., Aslanian, D., Olivet, J.-L., Contrucci, I., Matias, L., Géli, L., ... Unternehr, P. (2005). Geological constraints on the evolution of the Angolan margin based on reflection and refraction seismic data (Zaiango Project). *Geophysics Journal International*, *162*, 793–810. <https://doi.org/10.1111/j.1365-246X.2005.02668.x>
- Muravchik, M., Henstra, G. A., Eliassen, G. T., Gawthorpe, R. L., Leeder, M., Kranis, H., ... Andrews, J. (2019). Deep-water sediment transport patterns and basin floor topography in early rift basins: plio-pleistocene syn-rift of the corinth rift, Greece. *Basin Research*, *1*–29. <https://doi.org/10.1111/bre.12423>
- Mutti, E., & Normark, W. R. (1991). An integrated approach to the study of turbidite systems. In P. Weimer, & M. H. Link (Eds.), *Seismic facies and sedimentary processes of submarine fans and turbidite systems* (pp. 75–106). New York: Springer-Verlag.
- Niyazi, Y., Eruteya, O. E., Omosanya, K. O., Harishidayat, D., Johansen, S. E., & Waldmann, N. (2018). Seismic geomorphology of submarine channel-belt complexes in the pliocene of the levant basin. *Offshore Central Israel. Marine Geology*, *403*, 123–128.
- Olafiranye, K., Jackson, C. A. L., & Hodgson, D. M. (2013). The role of tectonics and mass-transport complex emplacement on upper slope stratigraphic evolution: A 3d seismic case study from offshore Angola. *Marine and Petroleum Geology*, *44*, 196–216. <https://doi.org/10.1016/j.marpetgeo.2013.02.016>
- Oluboyo, A. P., Gawthorpe, R. L., Bakke, K., & Hadler-Jacobsen, F. (2014). Salt tectonic controls on deep-water turbidite depositional systems: Miocene, southwestern lower Congo basin, offshore Angola. *Basin Research*, *26*, 597–620. <https://doi.org/10.1111/bre.12051>
- Ortiz-Karpf, A., Hodgson, D. M., Jackson, C. A. L., & McCaffrey, W. D. (2017). Influence of seabed morphology and substrate composition on mass-transport flow processes and pathways: insights from the Magdalena fan, offshore Colombia. *Journal of Sedimentary Research*, *87*, 189–209. <https://doi.org/10.2110/jsr.2017.10>
- Ortiz-Karpf, A., Hodgson, D. M., & McCaffrey, W. D. (2015). The role of mass-transport complexes in controlling channel avulsion and the subsequent sediment dispersal patterns on an active margin: The Magdalena fan, offshore Colombia. *Marine and Petroleum Geology*, *64*, 58–75. <https://doi.org/10.1016/j.marpetgeo.2015.01.005>
- Othman, A. A. A., Fathy, M., & Maher, A. (2016). Use of spectral decomposition technique for delineation of channels at solar gas discovery, offshore West Nile Delta, Egypt. *Egyptian Journal of Petroleum*, *25*, 45–51. <https://doi.org/10.1016/j.ejpe.2015.03.005>
- Patacci, M., Houghton, P. D. W., & McCaffrey, W. D. (2015). Flow behavior of ponded turbidity currents. *Journal of Sedimentary Research*, *85*, 885–902. <https://doi.org/10.2110/jsr.2015.59>
- Peel, F. J. (2014). The engines of gravity-driven movement on passive margins: quantifying the relative contribution of spreading vs. gravity sliding mechanisms. *Tectonophysics*, *633*, 126–142. <https://doi.org/10.1016/j.tecto.2014.06.023>
- Pichel, L. M., Finch, E., & Gawthorpe, R. L. (2019). The impact of pre-salt rift topography on salt tectonics: A discrete-element modeling approach. *Tectonics*, *38*, 1466–1488. <https://doi.org/10.1029/2018TC005174>
- Pichel, L. M., Jackson, C. A. L., Peel, F., & Dooley, T. P. (2020). Basalt Relief controls salt-tectonic structural style, são paulo plateau, Santos Basin, Brazil. *Basin Research*, *32*, 453–484. <https://doi.org/10.1111/bre.12375>
- Pichel, L. M., Peel, F., Jackson, C. A. L., & Huuse, M. (2018). Geometry and kinematics of salt-detached ramp syncline basins. *Journal of Structural Geology*, *115*, 208–230. <https://doi.org/10.1016/j.jsg.2018.07.016>
- Pinter, P. R., Butler, R. W. H., Hartley, A. J., Maniscalco, R., Baldassini, N., & Di Stefano, A. (2018). Tracking sand-fairways through a deformed turbidite system: The numidian (Miocene) of Central Sicily, Italy. *Basin Research*, *30*, 480–501. <https://doi.org/10.1111/bre.12261>
- Pirmez, C., Hiscou, R. N., & Kronen, J. K. (1997). Sandy turbidite successions at the base of channel-levee systems of the amazon fan revealed by fms logs and cores: Unraveling the facies architecture of large submarine fans. *Proceedings-Ocean Drilling Program Scientific Results*, *155*, 7–34.
- Posamentier, H. W. (2003). Depositional elements associated with a basin floor channel-levee system: Case study from the Gulf of Mexico. *Marine and Petroleum Geology*, *20*, 677–690. <https://doi.org/10.1016/j.marpetgeo.2003.01.002>
- Posamentier, H. W., & Kolla, V. (2003). Seismic geomorphology and stratigraphy of depositional elements in deep-water settings. *Journal of Sedimentary Research*, *73*, 367–388. <https://doi.org/10.1306/111302730367>
- Prather, B., Booth, J., Steffens, G., & Craig, P. (1998). Classification, lithologic calibration, and stratigraphic succession of seismic facies of Intraslope Basins, Deep-Water Gulf of Mexico. *AAPG Bulletin*, *82*, 701–728.
- Prather, B. E., Pirmez, C., Sylvester, Z., & Prather, D. S. (2012). Stratigraphic response to evolving geomorphology in a submarine apron perched on the upper niger delta slope. In B. E. Prather, M. E. Deptuck, D. C. Mohrig, vanHoorn B. & R. B. Wynn (Eds.), *Application of the Principles of Seismic Geomorphology to Continental-Slope and Base-of-Slope Systems: Case Studies From Seafloor and Near-Seafloor Analogue. SEPM Special Publication*, *99*, 145–161.
- Prélat, A., Covault, J. A., Hodgson, D. M., Fildani, A., & Flint, S. S. (2010). Intrinsic controls on the range of volumes, morphologies, and dimensions of submarine lobes. *Sedimentary Geology*, *232*, 66–76. <http://dx.doi.org/10.1016/j.sedgeo.2010.09.010>
- Quirk, D. G., Schödt, N., Lassen, B., Ings, S. J., Hsu, D., Hirsch, K. K., & Von Nicolai, C. (2012). Salt tectonics on passive margins: examples from santos, campos and Kwanza Basins. In G. I. Alsop, S. G. Archer, A. J. Hartley, N. T. Grant & R. Hodgkinson (Eds.), *Salt tectonics, sediments, prospectivity. Geological Society, London, Special Publications*, *363*, 207–244.
- Ravnås, R., & Steel, R. J. (1998). Architecture of marine rift-basin successions. *AAPG Bulletin*, *82*, 110–146.
- Rodriguez, C. R., Jackson, C. A. L., Bell, R. E., Rotevatn, A., & Francis, M. (2020). *Deep-Water Reservoir Distribution on a Salt-Influenced Slope*. Offshore Brazil Santos Basin.

- Royo, L. A., & Escalona, A. (2018). Controls on minibasin infill in the Nordkapp Basin: Evidence of complex triassic syndepositionary deposition influenced by salt tectonics. *AAPG Bulletin*, *102*, 1239–1272. <https://doi.org/10.1306/0926171524316523>
- Serié, C., Huuse, M., Schødt, N. H., Brooks, J. M., & Williams, A. (2017). Subsurface fluid flow in the deep-water Kwanza Basin, offshore Angola. *Basin Research*, *29*, 149–179. <http://dx.doi.org/10.1111/bre.12169>
- Smith, R. U. (2004) Silled sub-basins to connected tortuous corridors: Sediment distribution systems on topographically complex sub-aqueous slopes. In S. A. Lomas & P. Joseph (Eds.), *Confined turbidite systems. Geological Society, London, Special Publications*, *222*, 23–44.
- Straub, K. M., & Mohrig, D. (2009). Constructional canyons built by sheet-like turbidity currents: observations from offshore Brunei Darussalam. *Journal of Sedimentary Research*, *79*, 24–39. <https://doi.org/10.2110/jsr.2009.006>
- Tari, G., Molnar, J., & Ashton, N. (2003) Examples of Salt tectonics from West Africa: A comparative approach. In W.U. Mohriak, A. Danforth, P.J. Post, D.E. Brown, G.C. Tari, M. Nemcok & S.T. Sinha (Eds.), *Conjugate Divergent Margins. Geological Society, London, Special Publications*, *207*, 85–104.
- Tinterri, R., Laporta, M., & Ogata, K. (2017). Asymmetrical cross-current turbidite facies tract in a structurally-confined Mini-Basin (Priabonian-Rupelian, Ranzano Sandstone, Northern Apennines, Italy). *Sedimentary Geology*, *352*, 63–87. <https://doi.org/10.1016/j.sedgeo.2016.12.005>
- Valle, P. J., Gjelberg, J. G., & Helland-Hansen, W. (2001). Tectonostratigraphic development in the eastern lower congo basin, offshore Angola, West Africa. *Marine and Petroleum Geology*, *18*, 909–927.
- Van Andel, T. H., & Komar, P. D. (1969). Ponded sediments of the mid-atlantic ridge between 22 and 23 north latitude. *GSA Bulletin*, *80*, 1163–1190. [https://doi.org/10.1130/0016-7606\(1969\)80\[1163:P-SOTMR\]2.0.CO;2](https://doi.org/10.1130/0016-7606(1969)80[1163:P-SOTMR]2.0.CO;2)
- Wagner, B. H. III, & Jackson, M. P. (2011). Viscous flow during salt welding. *Tectonophysics*, *510*, 309–326. <https://doi.org/10.1016/j.tecto.2011.07.012>
- Ward, N. I. P., Alves, T. M., & Blenkinsop, T. G. (2017). Differential Compaction over Late Miocene Submarine Channels in SE Brazil: Implications for Trap Formation. *GSA Bulletin*, *130*, 208–221. <https://doi.org/10.1130/B31659.1>
- Wu, N., Jackson, C. A. L., Johnson, H. D., Hodgson, D. M., & Nugraha, H. D. (2020). Mass-Transport Complexes (MTCs) Document Subsidence Patterns in a Northern Gulf of Mexico Salt Minibasin. *Basin Research*, 1–28. <https://doi.org/10.1111/bre.12429>
- Wynn, R. B., Kenyon, N. H., Masson, D. G., Stow, D. A., & Weaver, P. P. (2002). Characterization and Recognition of Deep-water Channel-lobe Transition Zones. *AAPG Bulletin*, *86*, 1441–1462.
- Zhao, X., Qi, K., Patacci, M., Tan, C., & Xie, T. (2019). Submarine Channel Network Evolution above an Extensive Mass-Transport Complex: A 3d Seismic Case Study from the Niger Delta Continental Slope. *Marine and Petroleum Geology*, *104*, 231–248. <https://doi.org/10.1016/j.marpetgeo.2019.03.029>

**How to cite this article:** Howlett DM, Gawthorpe RL, Ge Z, Rotevatn A, Jackson CA-L. Turbidites, topography and tectonics: Evolution of submarine channel-lobe systems in the salt-influenced Kwanza Basin, offshore Angola. *Basin Res.* 2020;00:1–35. <https://doi.org/10.1111/bre.12506>